MARTIN MARIETTA ENERGY SYSTEMS LIBRARIES

3 4456 0280509 8

ORNL/TM-10810

ornl

OAK RIDGE NATIONAL LABORATORY

MARTIN MARIETTA

An Approximation for Black-Body X-Ray Transport in Air

C. M. Haaland
R. T. Santoro
J. M. Barnes

OAK RIDGE NATIONAL LABORATORY
CENTRAL RESEARCH LIBRARY
CIRCULATION SECTION
4500N ROOM 175
LIBRARY LOAN COPY
DO NOT TRANSFER TO ANOTHER PERSON
If you wish someone else to see this report, send in name with report and the library will arrange a loan.

OPERATED BY
MARTIN MARIETTA ENERGY SYSTEMS, INC.
FOR THE UNITED STATES
DEPARTMENT OF ENERGY

Printed in the United States of America. Available from
National Technical Information Service
U.S. Department of Commerce
5285 Port Royal Road, Springfield, Virginia 22161
NTIS price codes—Printed Copy: A03; Microfiche A01

This report was prepared as an account of work sponsored by an agency of the United States Government. Neither the United States Government nor any agency thereof, nor any of their employees, makes any warranty, express or implied, or assumes any legal liability or responsibility for the accuracy, completeness, or usefulness of any information, apparatus, product, or process disclosed, or represents that its use would not infringe privately owned rights. Reference herein to any specific commercial product, process, or service by trade name, trademark, manufacturer, or otherwise, does not necessarily constitute or imply its endorsement, recommendation, or favoring by the United States Government or any agency thereof. The views and opinions of authors expressed herein do not necessarily state or reflect those of the United States Government or any agency thereof.

ORNL/TM-10810

Engineering Physics and Mathematics Division

AN APPROXIMATION FOR BLACK-BODY X-RAY TRANSPORT IN AIR

C. M. Haaland
R. T. Santoro
J. M. Barnes*

Oak Ridge National Laboratory
Post Office Box 2008
Oak Ridge, Tennessee 37831

*Computing and Telecommunications Division

DATE PUBLISHED — August 1988

Prepared by
Oak Ridge National Laboratory
Oak Ridge, Tennessee 37831
operated by
MARTIN MARIETTA ENERGY SYSTEMS, INC.
for the
U.S. DEPARTMENT OF ENERGY
under Contract No. DE-AC05-84OR21400

MARTIN MARIETTA ENERGY SYSTEMS LIBRARIES

3 4456 0280509 8

CONTENTS

ABSTRACT v
1. INTRODUCTION 1
2. METHODOLOGY 3
3. CALIBRATION AND RESULTS 7
4. CONCLUSIONS 35
REFERENCES 37

ABSTRACT

A simplified method is presented for approximating the air-transported x-ray spectrum from nuclear detonations in the atmosphere. Computational time is reduced such that a desk-top computer can provide results that match, within $\pm 10\%$ for a wide range of conditions, Monte Carlo results which require about the same computation time on a Cray. The method consists of 1) representing the black-body continuous spectrum by discrete emission windows, 2) consulting tables of photon buildup factors for the discrete emission energies, 3) unfolding the buildup photons by using air kerma response functions and an assumption for redistributing these photons to windows of lower energy, and 4) applying cutoff and weighting factors to improve the correlation with the Monte Carlo benchmark calculations.

1. INTRODUCTION

This paper describes a simplified method for approximating the air-transported x-ray spectrum from nuclear detonations in the atmosphere.* The early fireball of a nuclear detonation emits intense x-ray radiation that can be approximated by the spectrum from a black-body at a temperature of around 10^7–10^8 K.[1] A number of procedures have been devised [2–5] for calculating the transport of photons and neutrons in various media. Tables have been prepared [6–9] that provide the x-ray flux at a distance R from a nuclear detonation in the atmosphere for a limited set of parameters. The method described here reduces computational time such that a desk-top computer can provide results that match, within $\pm 10\%$ for a wide range of conditions, Monte Carlo[5] results which require about the same computation time on a Cray.

The method consists of 1) representing the black-body continuous spectrum by discrete emission windows, 2) consulting tables of photon buildup factors for the discrete emission energies, 3) unfolding the buildup photons by using air kerma response functions and an assumption for redistributing these photons to windows of lower energy, and 4) applying cutoff and weighting factors to improve the correlation with the Monte Carlo benchmark calculations.

* This work was sponsored by the U.S. Air Force, Aeronautical Systems Division, Air Force Wright Aeronautical Laboratories, Flight Dynamics Division, Advanced Development Projects Office. Mr. S. D. Thompson was the responsible Air Force project engineer. The work was performed during CY 1987.

2. METHODOLOGY

The distribution of radiated power P_ν in cal/cm^2 for a black-body at temperature T as a function of the photon frequency ν at a distance D cm *in vacuum* from a nuclear detonation of yield W kilotons with the fraction F_x going into x-ray production is given by

$$P_\nu d\nu = \frac{10^{12} W F_x J_\nu d\nu}{4\pi D^2 \sigma T^4} \quad , \tag{1}$$

where $J_\nu d\nu$ represents the Planck emission equation in terms of the photon frequency and σ is the Stefan-Boltzmann constant.

It was assumed for this approximation that the black body spectrum can be represented adequately by 15 discrete frequencies, one of them being the frequency $\nu_m = 2.8214kT/h$, at which the radiant power is a maximum. The other 14 frequencies were specified by dividing the Planck spectrum into uniform bands representing 1/10, 1/20, and 1/40th of the total power emitted, the narrow bands being used at the ends of the spectrum. The Planck emission equation was integrated numerically to higher and lower values from the frequency where the radiant power is a maximum in order to find the discrete emission frequencies and band widths that were used to represent the continuous power spectrum. These frequencies and band widths are shown in Table 1. With this scheme, the specification of the black-body temperature, T, uniquely specifies the 15 discrete representative frequencies ν_i for the entire spectrum, as well as the fractional power f_{pi} emitted at the ith frequency.

For a specific problem, the uncollided flux at the desired range and the number of mean free paths is computed for each discrete frequency. For problems involving other than zero angle between the source and detector, it is assumed that the integrated air mass per unit area along the source-detector vector is uniformly distributed along the vector. The effect of this assumption was not checked, but it should not be significant as long as the range is less than an atmospheric scale-height.

Buildup factors for energy flux are determined by interpolation from a matrix of data computed for air kerma response as a function of photon energy and number of mean free paths for a point source in an infinite uniform air medium.[10] The buildup factor B_i for the ith discrete emission frequency is defined by[11]

$$B_i = \frac{R_i}{R_i^{un}} = \frac{\int_0^{E_i} dE\ A(E)\phi^{tot}(E)}{A(E_i)\phi^{un}(E_i)} \quad , \tag{2}$$

Table 1. Representation of Black-Body

Emission Spectrum by 15 Discrete Emission Energies

		Conversion Numbers, N*		
Window Number	Percent of Total Power	Range of Spectral Window	Discrete Emission Energy	Width of Spectral Window
1	4.6	2.75042–3.15539	3.15539	0.40497
2	5	2.34632–2.75042	2.51554	0.40410
3	10	1.91842–2.34632	2.10060	0.42790
4	10	1.64444–1.91842	1.77068	0.27398
5	10	1.43122–1.69444	1.53270	0.21322
6	10	1.24847–1.43122	1.33715	0.18275
7	10	1.08117–1.24847	1.16359	0.16730
8	10	0.91881–1.08117	1.00000	0.16236
9	10	0.75008–0.91881	0.83615	0.16873
10	5	0.65760–0.75008	0.70490	0.09248
11	5	0.55306–0.65760	0.60739	0.10454
12	2.5	0.49259–0.55306	0.52378	0.06047
13	2.5	0.42199–0.49259	0.45895	0.07060
14	2.5	0.33110–0.42199	0.38029	0.09089
15	2.9	0.20000–0.33110	0.26000	0.13110

*Photon energies are given by

$$E = 2.432 \times 10^{-7} NT, \qquad (keV)$$

where N is a conversion number from the table above and T is the black-body temperature in K.

where R_i^{un} is the reading of an idealized ionization chamber with no walls and air response characteristics to the uncollided flux, and R_i is the reading in response to the actual photon flux, which includes inscattered photons due to Compton scattering. $A(E)$ is the response function[11], $\phi^{un}(E_i)$ is the uncollided flux of photons with the discrete energy E_i, and $\phi^{tot}(E)$ is the total flux of all photon energies, including the uncollided flux of energy E_i and photons of lower energy resulting from incoherent scattering.

We assume that the integral in Eq. (2) taken over all energies is sufficiently represented by the sum over the appropriate discrete frequencies used to represent the black-body radiation, the appropriate frequencies including the frequency ν_i and all lower frequencies. Furthermore, we assume, initially, that inscattered photons are distributed equally throughout all transmitted frequencies below the incident photon frequency. These assumptions allow Eq. (2) to be solved for the total scattered flux ϕ_i^{sc} resulting from the ith discrete emission, namely,

$$\Phi_i^{sc} = \frac{(B_i - 1)R_i^{un}}{\sum_{j=1}^{i} A(E_j)\, W_j/S} \quad , \tag{3}$$

in which W_j is the window width in frequency for the jth window, and S is the sum of the frequencies over all transmittable windows. From this solution, the scattered flux contribution to window j is simply given by

$$\Phi_{i,j}^{sc} = \Phi_i^{sc}\, W_j/S \quad . \tag{4}$$

In anticipation that the assumption of equal distribution of scattered photons through lower frequencies may not be valid either throughout the range of pertinent black-body temperatures or throughout a range of values for the mean free path or for a combination of these factors, a dimensionless form factor was developed to modify the window width, given by

$$W_i = \left[\frac{(E_i/E_0)^{2.5}}{B_i}\right]^G e^{-M_i/2} \quad , \tag{5}$$

where B_i is the buildup factor obtained by extrapolation from a table[10], E_i is the energy of photons from the ith window, E_0 is the cutoff energy for transmission, taken to be 1 keV, and M_i is the number of mean free paths for the photon in the problem under consideration. The value of G was determined by comparing the approximation results with those obtained with a Monte Carlo calculation.

3. CALIBRATION AND RESULTS

Monte Carlo benchmarks were calculated for 24 cases, namely, black-body temperatures of 4×10^7 and 4×10^8 K (3.45 and 34.5 keV), atmospheric densities of 4.42×10^{-5}, 1.71×10^{-5}, 1.78×10^{-6}, and 2.74×10^{-7} g/cm^3 (corresponding to altitudes of 80, 100, 150, and 200 kft, respectively), and ranges of 1, 2, and 4 km. The MCNP code[5] was used on a Cray computer, requiring about 15 seconds machine time per run. Both methods of calculation used photon mass attenuation coefficients included within the MCNP program. The approximation calculation used energy absorption coefficients from Hubbell[12] to calculate the response functions.

For each case, a value of G was found that provided approximately the best match between the two results, using total energy flux, total photon flux, and the number of windows in which the photon flux differences were less than 20%. It was found that the optimum G plotted against the parameter $P = B_1 M_1 E_1$ (E in keV) for each case could be represented by two straight lines on exponential graph paper, thus specifying optimum G values given by the equations.

$$G = 0.7744 \ln(207.9/P) \quad \text{For} \quad P < 200 \tag{6a}$$

and

$$G = 0.2667 \ln(178.7/P) \quad \text{For} \quad P \geq 200 \ . \tag{6b}$$

Comparisons of the integrated energies and photon fluxes for the 24 cases are shown in Figures 1 and 2, respectively. The percent deviations of the results of the approximation from those of the MCNP calculation are less than 10% for 20 out of 24 cases for the energy (Figure 1), and for 19 out of 24 cases for the flux (Figure 2). The approximation does not provide good results when over half of the emission channels become nontransmitting due to a large number of mean free paths (>10).

Detailed spectral comparisons between the results of the approximation and the Monte Carlo runs are illustrated in Figures 3–26.

For the lower temperature black-body spectrum (4×10^7 K), the most energetic source photons have an energy of only 30.7 keV, and range down to 1.4 keV. Consequently, photoelectric absorption of photons dominates the attenuation, and low energy photons are strongly absorbed, as illustrated in Figures 3–14.

For the higher temperature spectrum (4×10^8 K), the photon energies range from 14–307 keV, spanning the energy range over which the incoherent scattering cross section has a maximum (30–50 keV), and also the range over which buildup factors have maxima (80–100 keV).[10] In this case, redistribution of the buildup photons provides significant modification of the resultant spectra, as indicated by results of both methods in Figures 15–20.

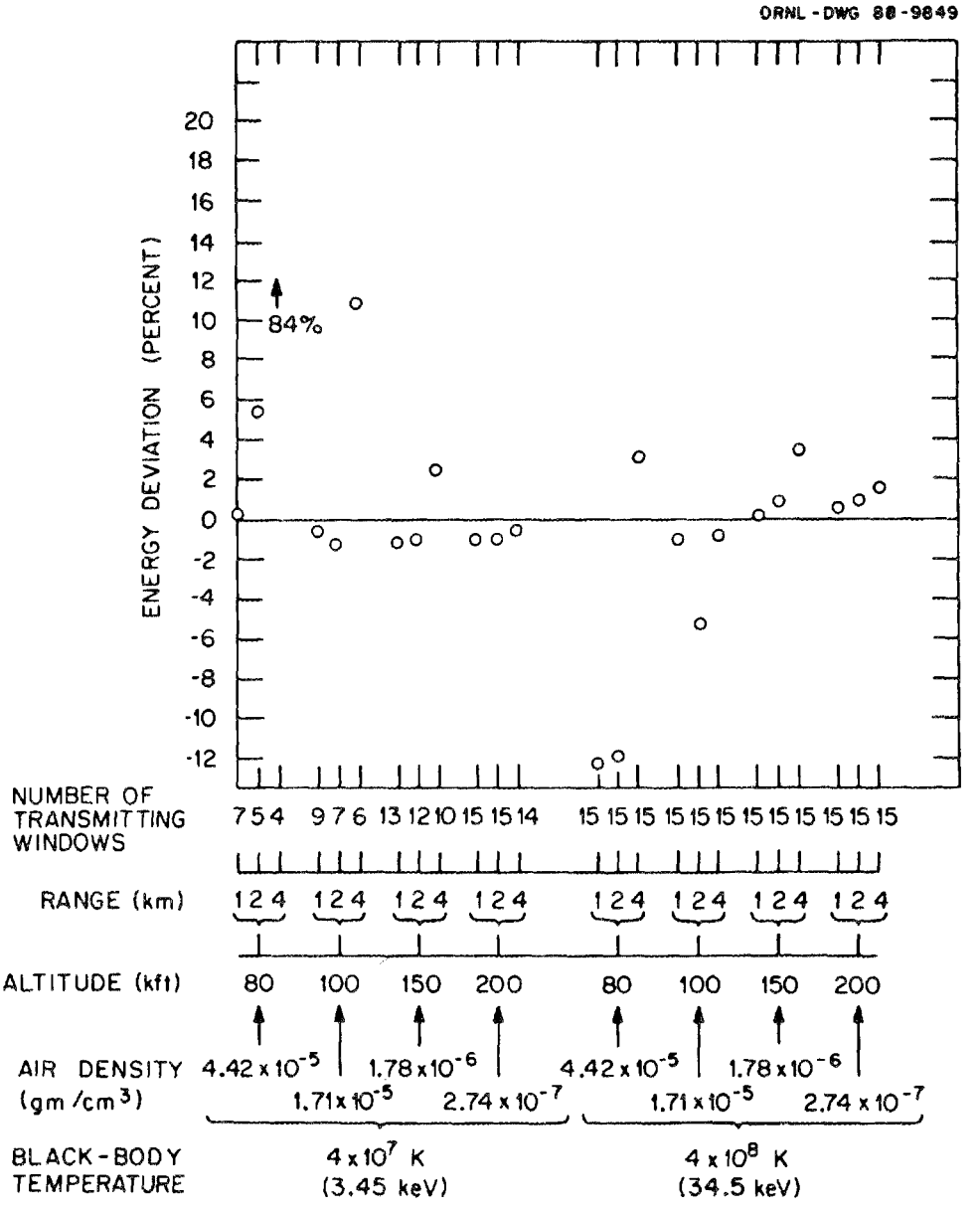

Figure 1. Deviation (percent) of approximation results from Monte Carlo results for the total energy delivered for 24 cases.

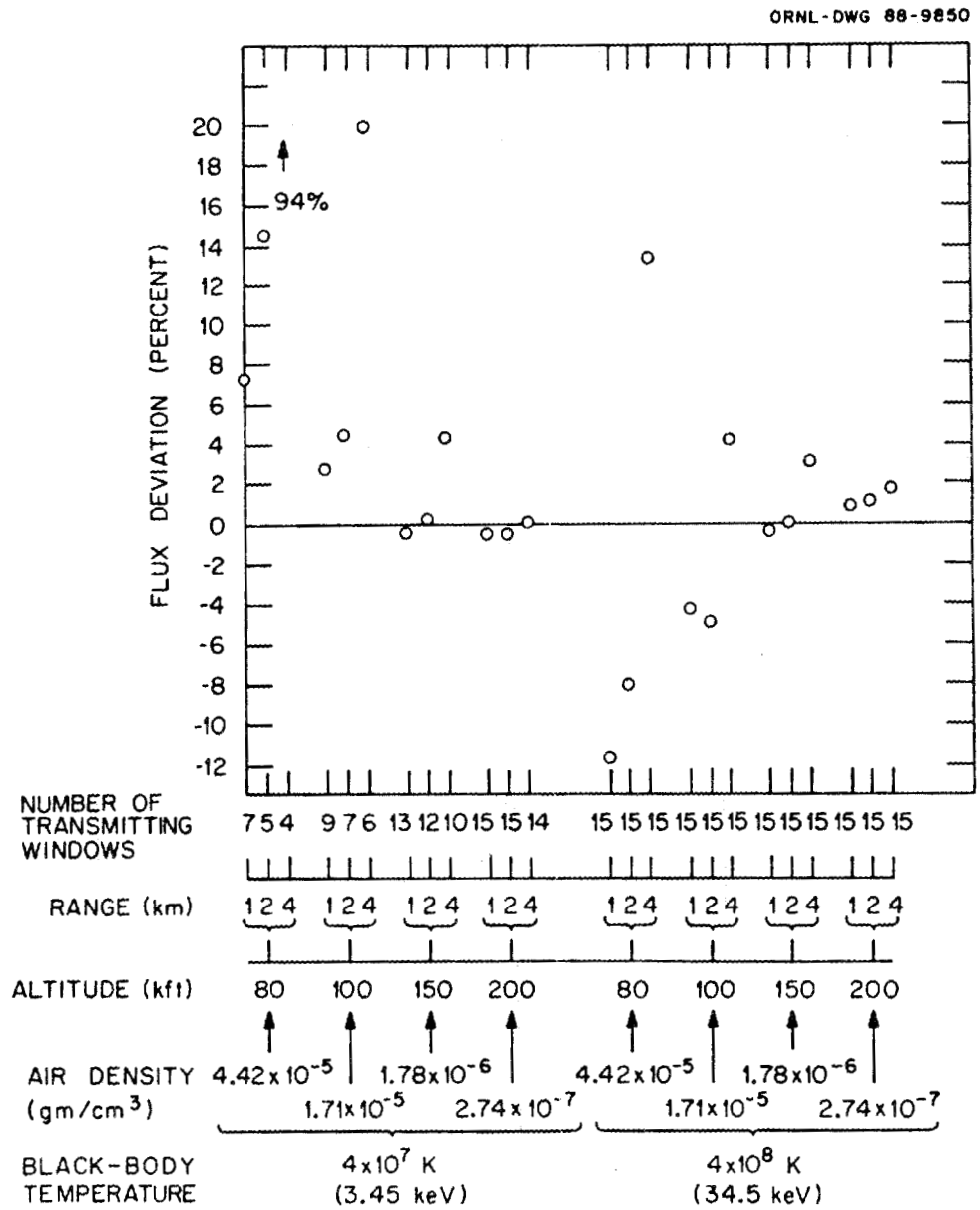

Figure 2. Deviation (percent) of approximation results from Monte Carlo results for the total photon flux delivered for 24 cases.

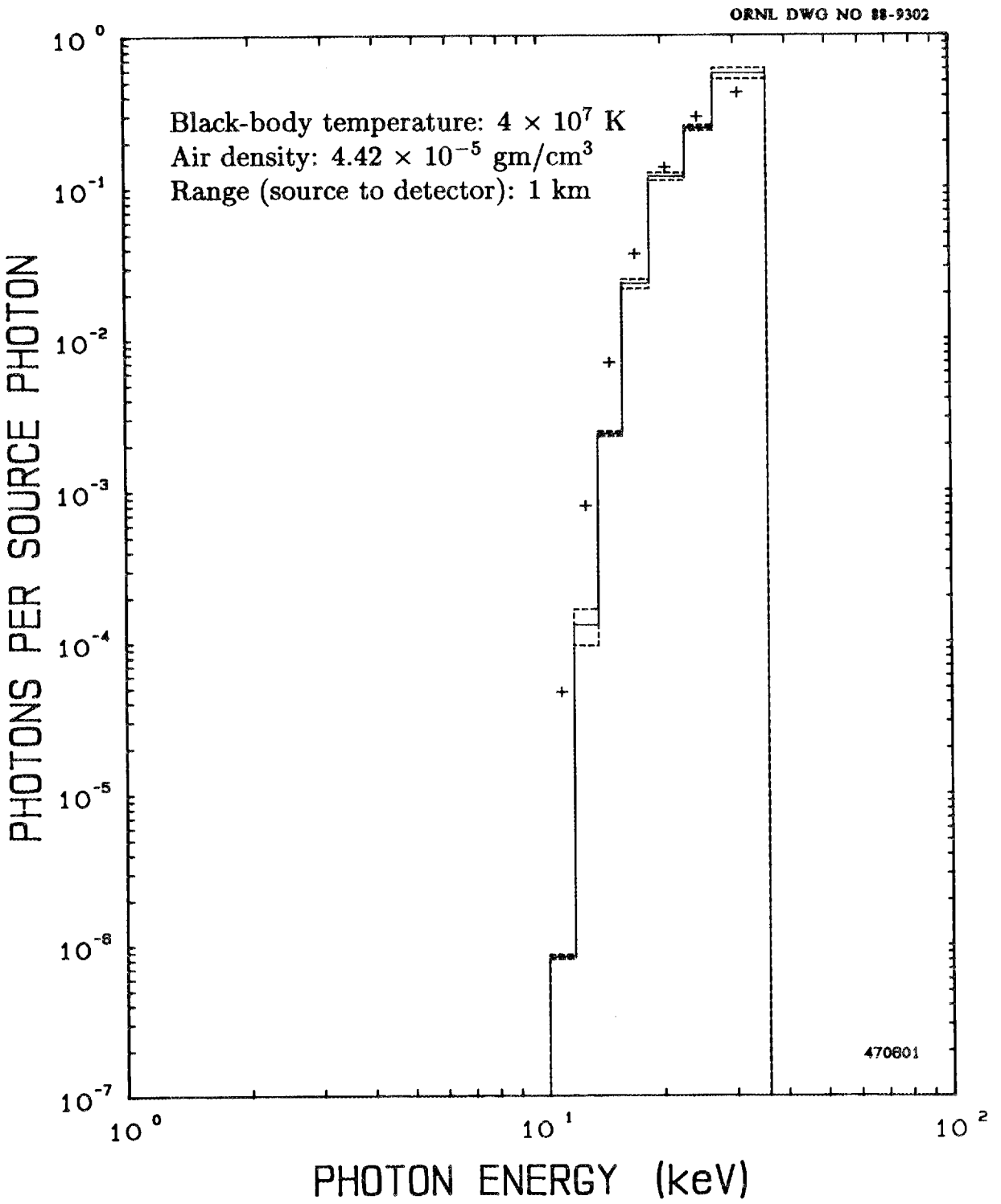

Figure 3. Detailed spectral comparisons of results from the approximation method (plus signs) with the Monte Carlo method (histogram with error limits indicated) for the case indicated on the figure.

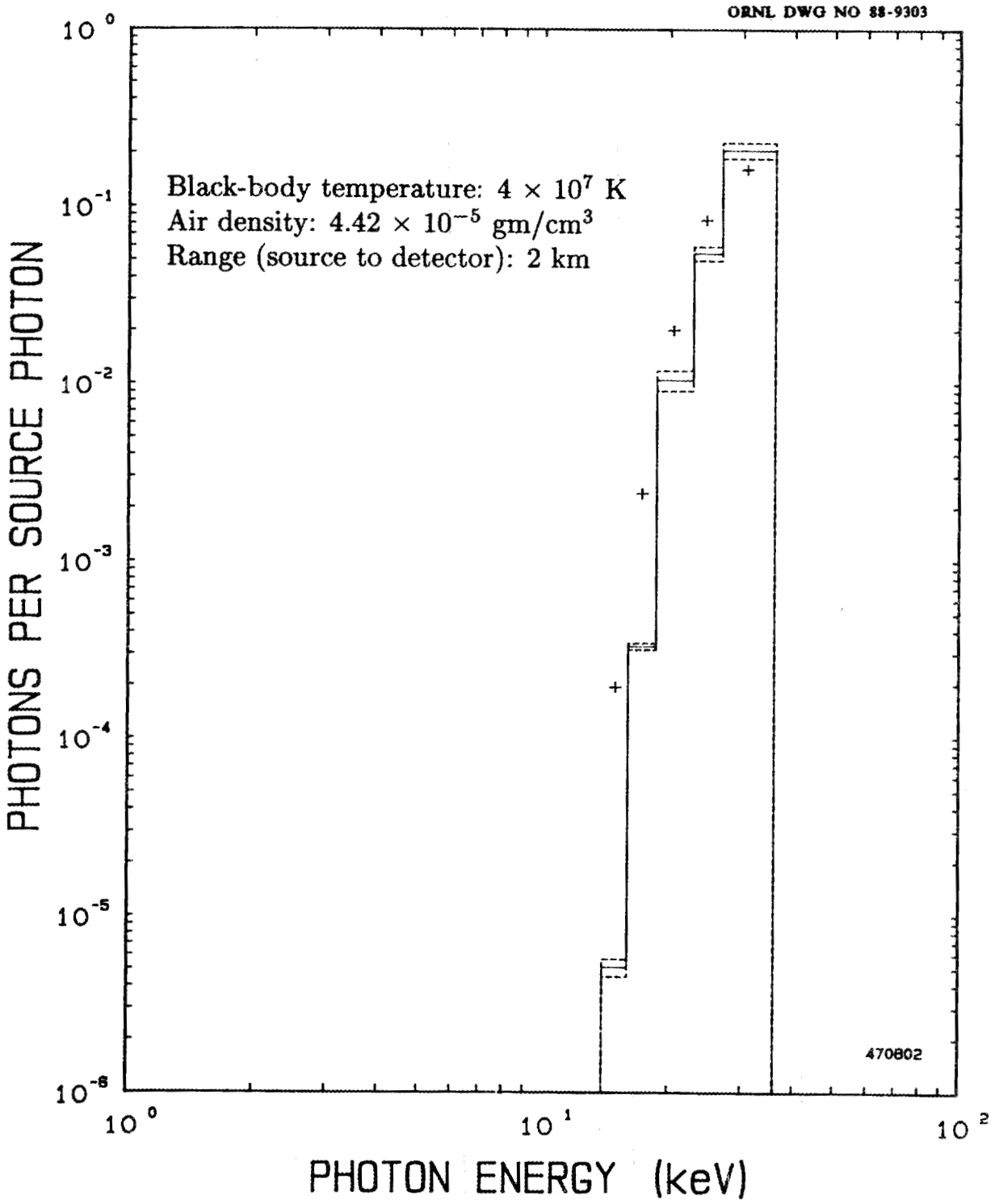

Figure 4. Detailed spectral comparisons of results from the approximation method (plus signs) with the Monte Carlo method (histogram with error limits indicated) for the case indicated on the figure.

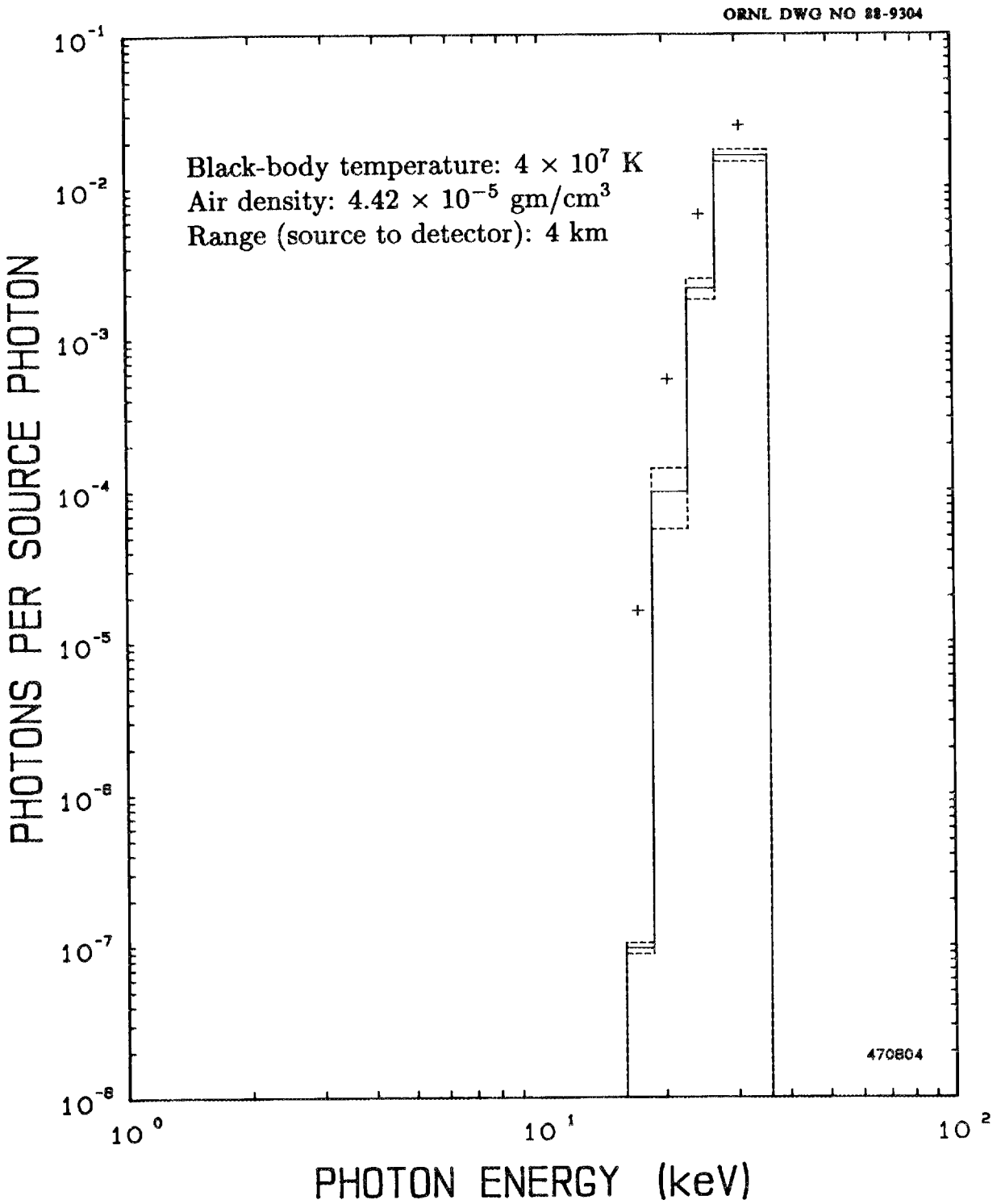

Figure 5. Detailed spectral comparisons of results from the approximation method (plus signs) with the Monte Carlo method (histogram with error limits indicated) for the case indicated on the figure.

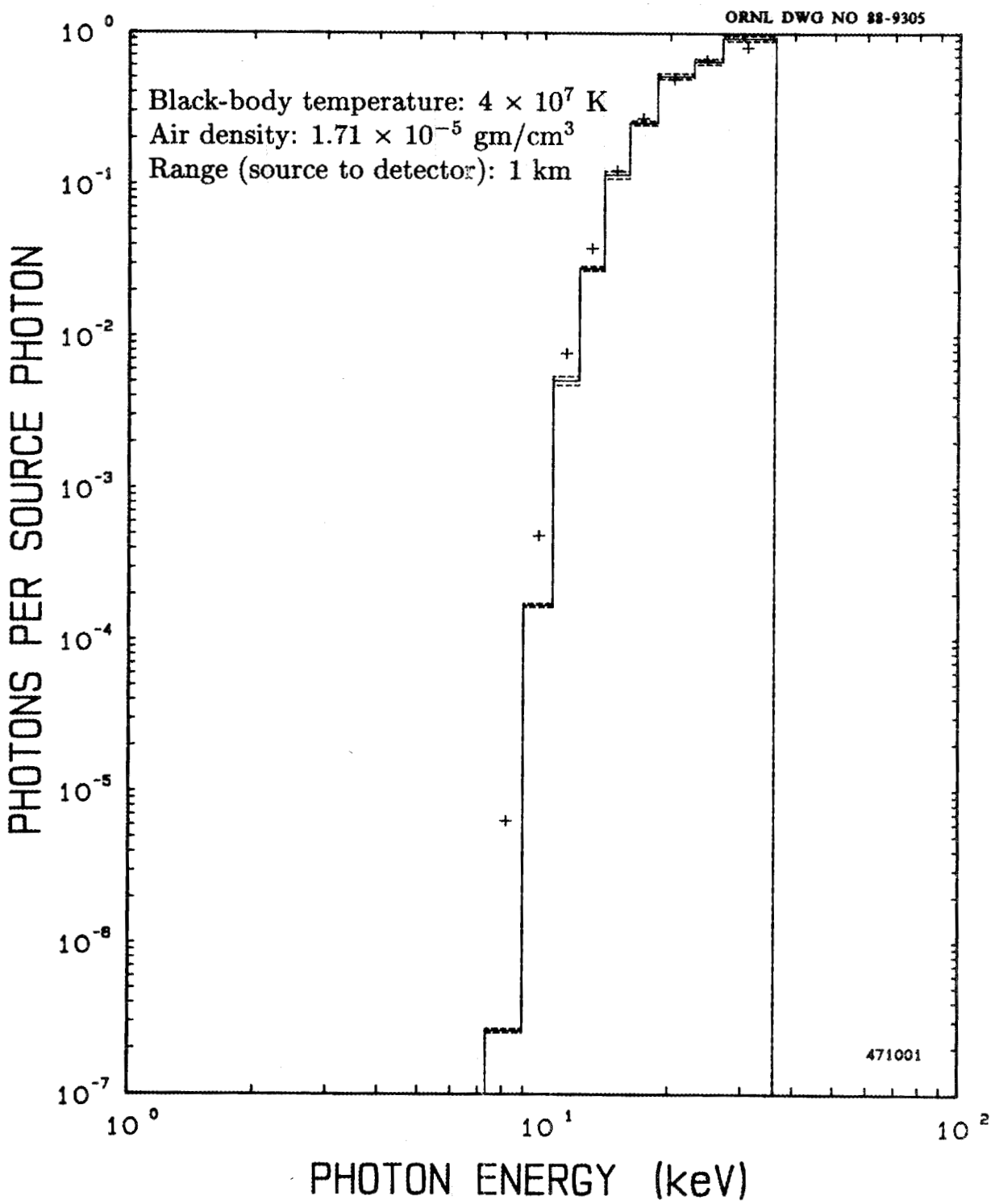

Figure 6. Detailed spectral comparisons of results from the approximation method (plus signs) with the Monte Carlo method (histogram with error limits indicated) for the case indicated on the figure.

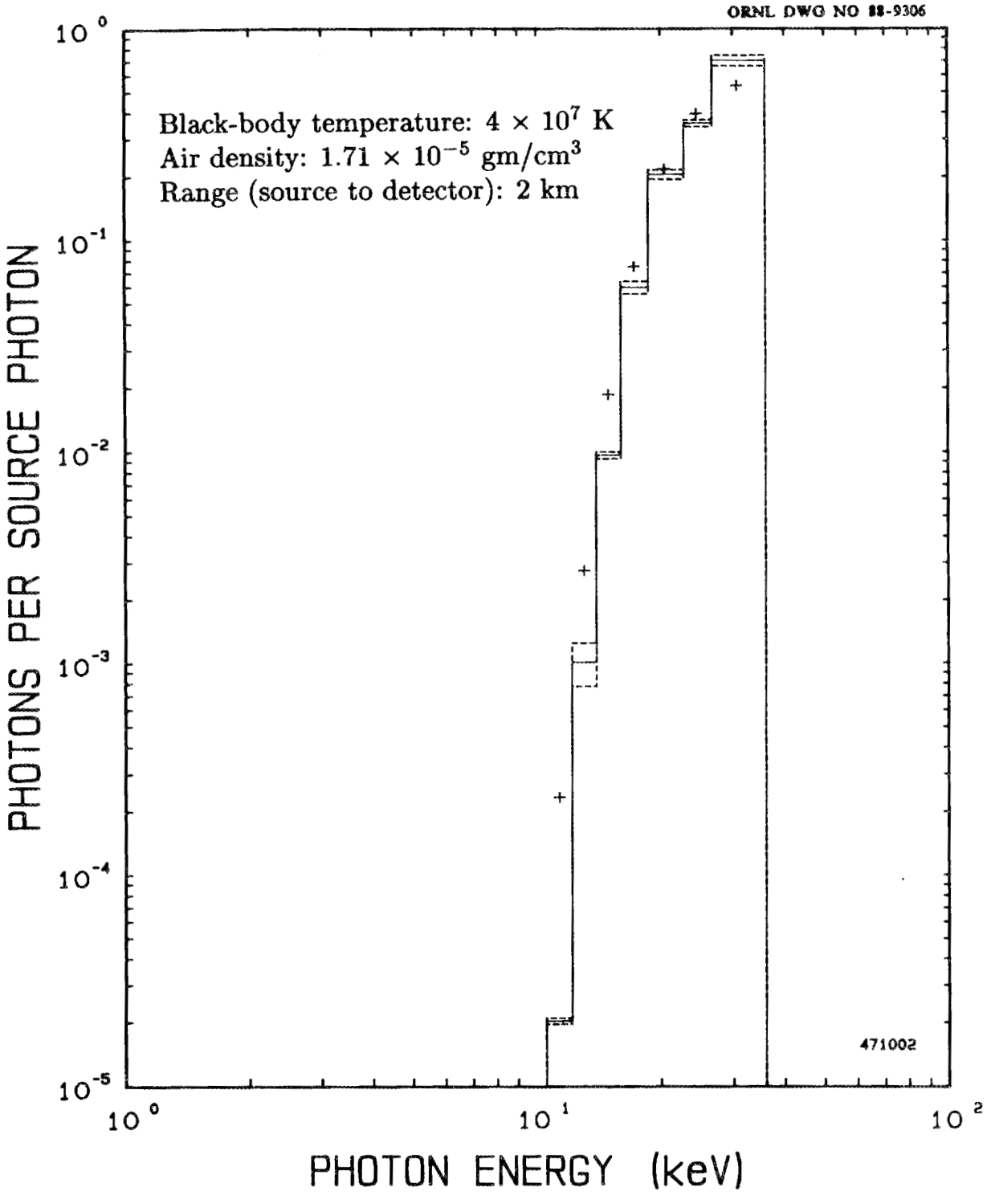

Figure 7. Detailed spectral comparisons of results from the approximation method (plus signs) with the Monte Carlo method (histogram with error limits indicated) for the case indicated on the figure.

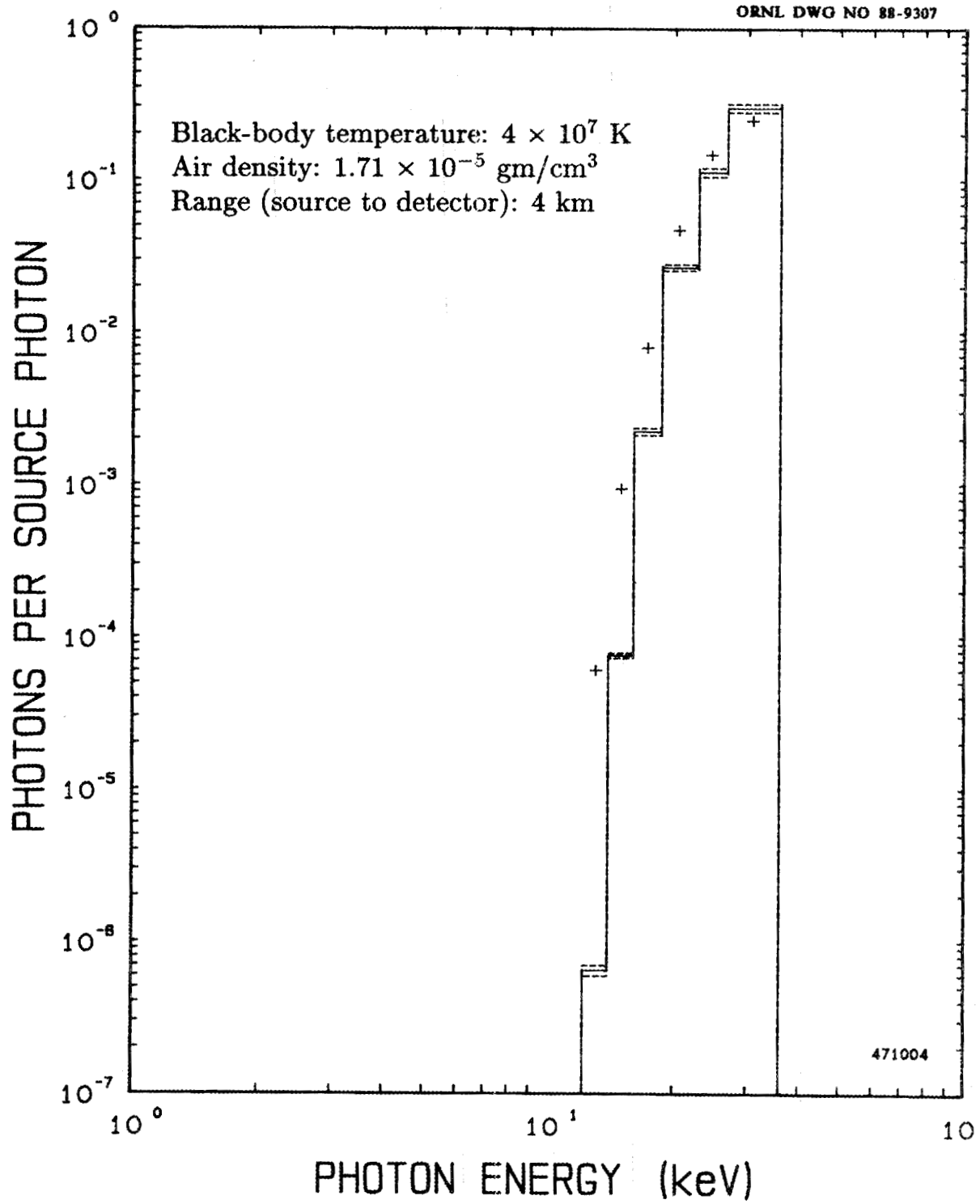

Figure 8. Detailed spectral comparisons of results from the approximation method (plus signs) with the Monte Carlo method (histogram with error limits indicated) for the case indicated on the figure.

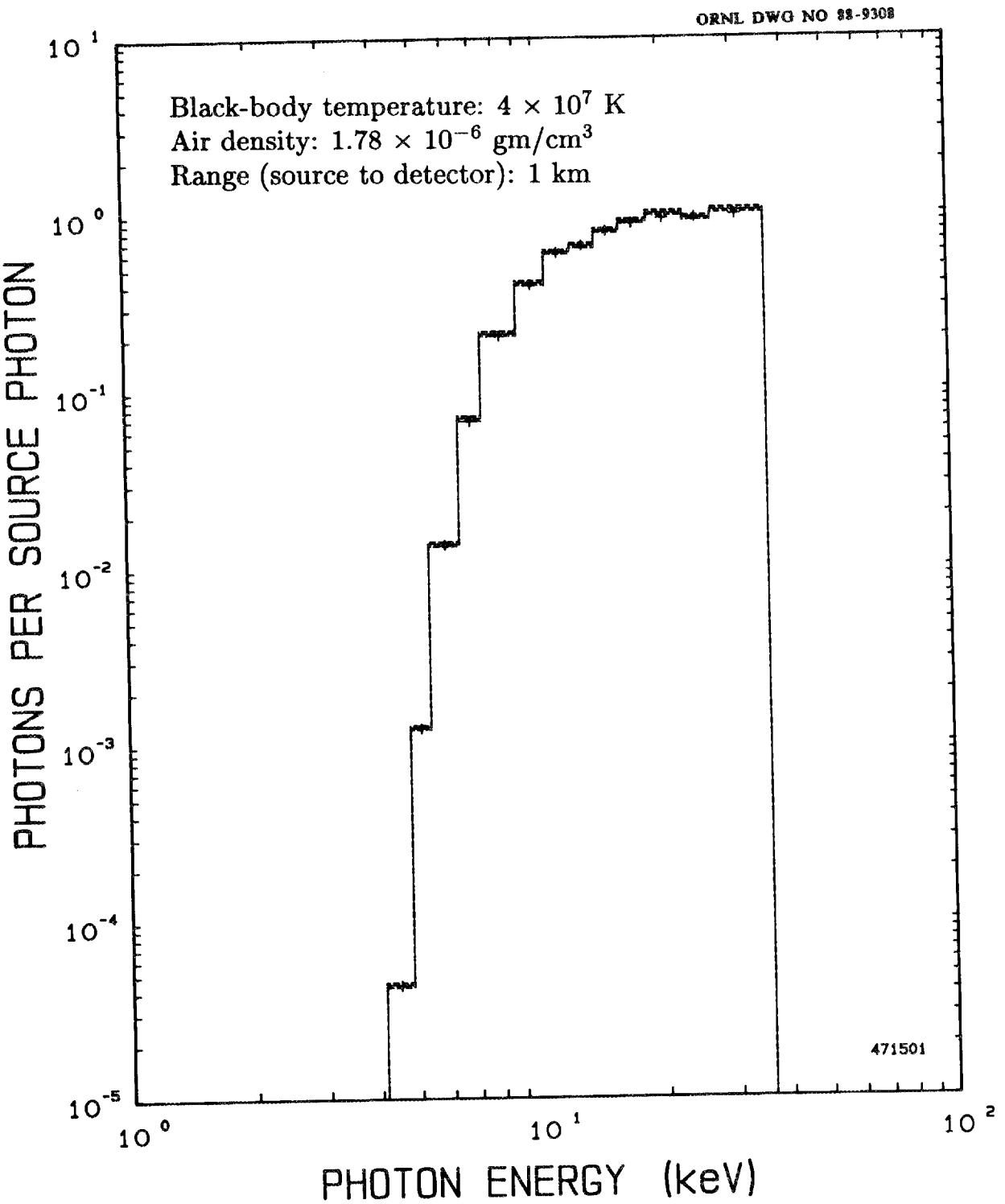

Figure 9. Detailed spectral comparisons of results from the approximation method (plus signs) with the Monte Carlo method (histogram with error limits indicated) for the case indicated on the figure.

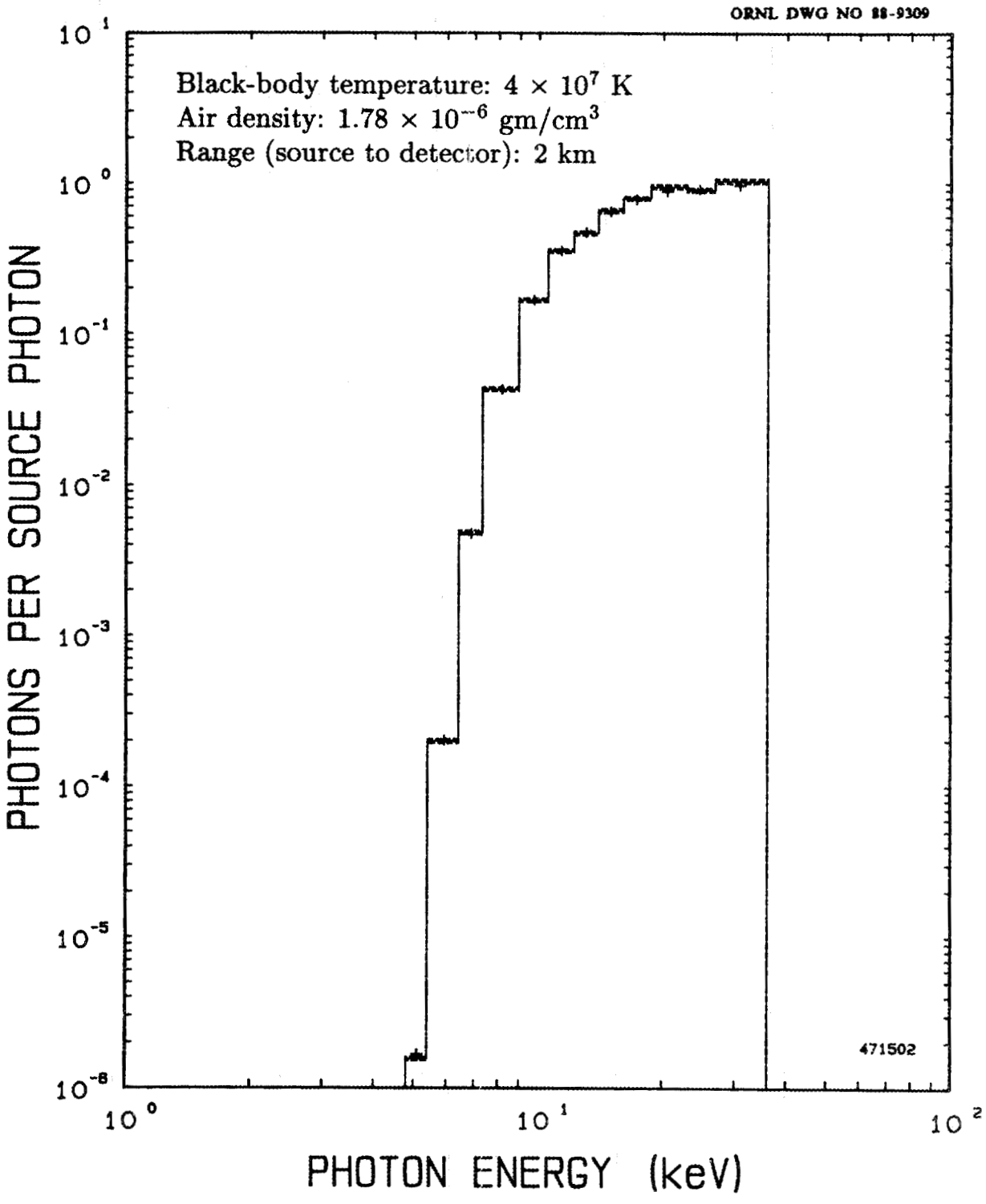

Figure 10. Detailed spectral comparisons of results from the approximation method (plus signs) with the Monte Carlo method (histogram with error limits indicated) for the case indicated on the figure.

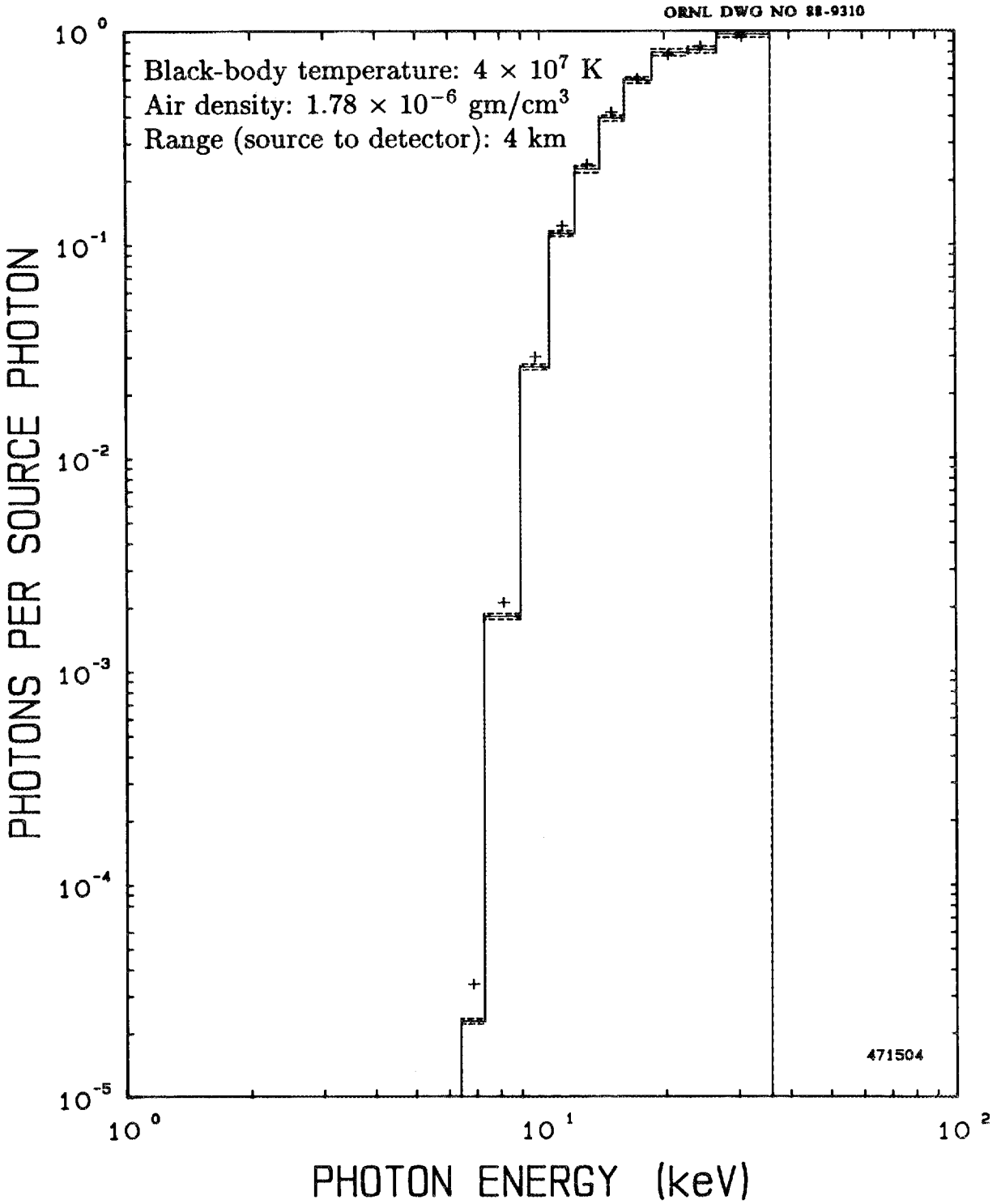

Figure 11. Detailed spectral comparisons of results from the approximation method (plus signs) with the Monte Carlo method (histogram with error limits indicated) for the case indicated on the figure.

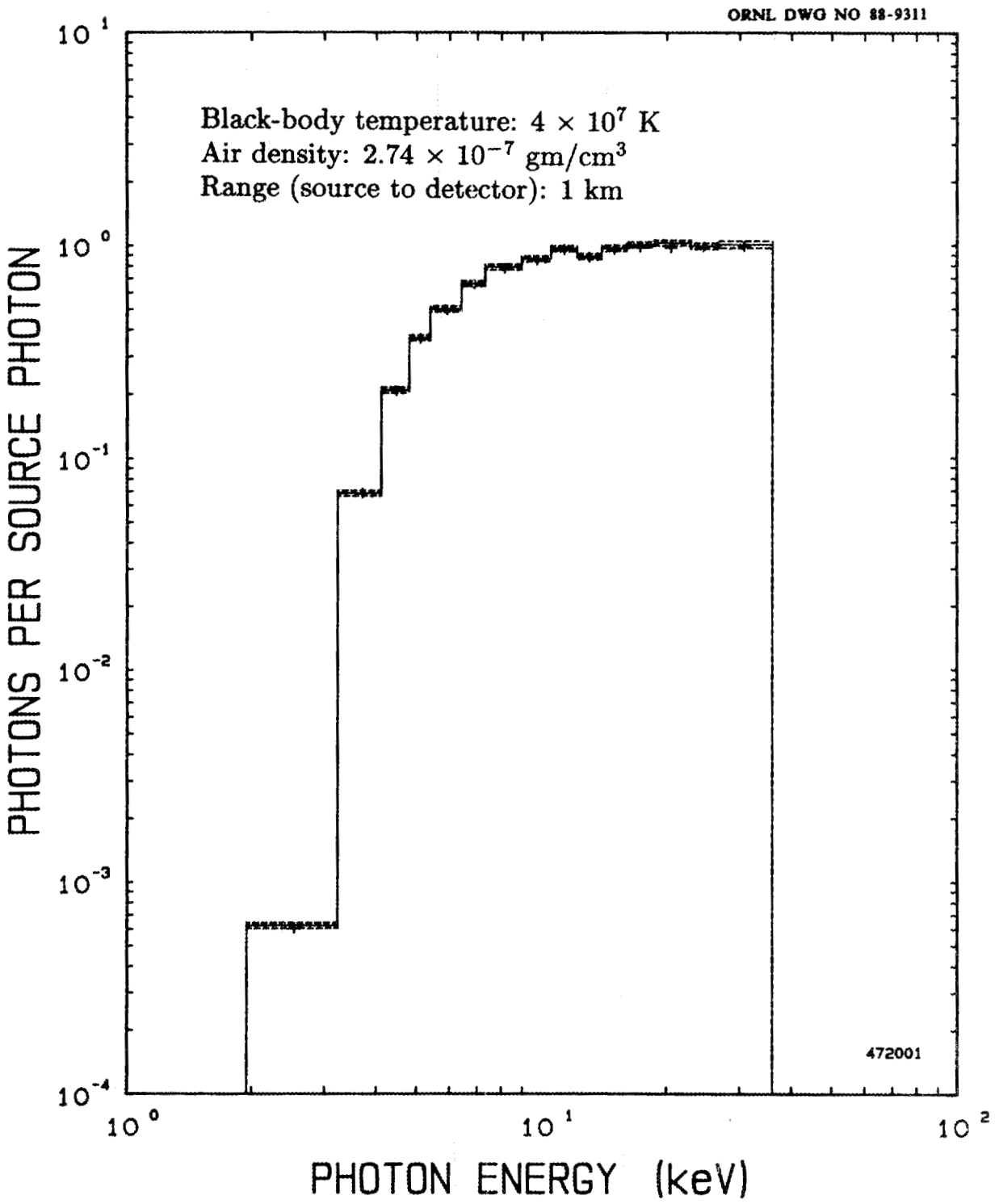

Figure 12. Detailed spectral comparisons of results from the approximation method (plus signs) with the Monte Carlo method (histogram with error limits indicated) for the case indicated on the figure.

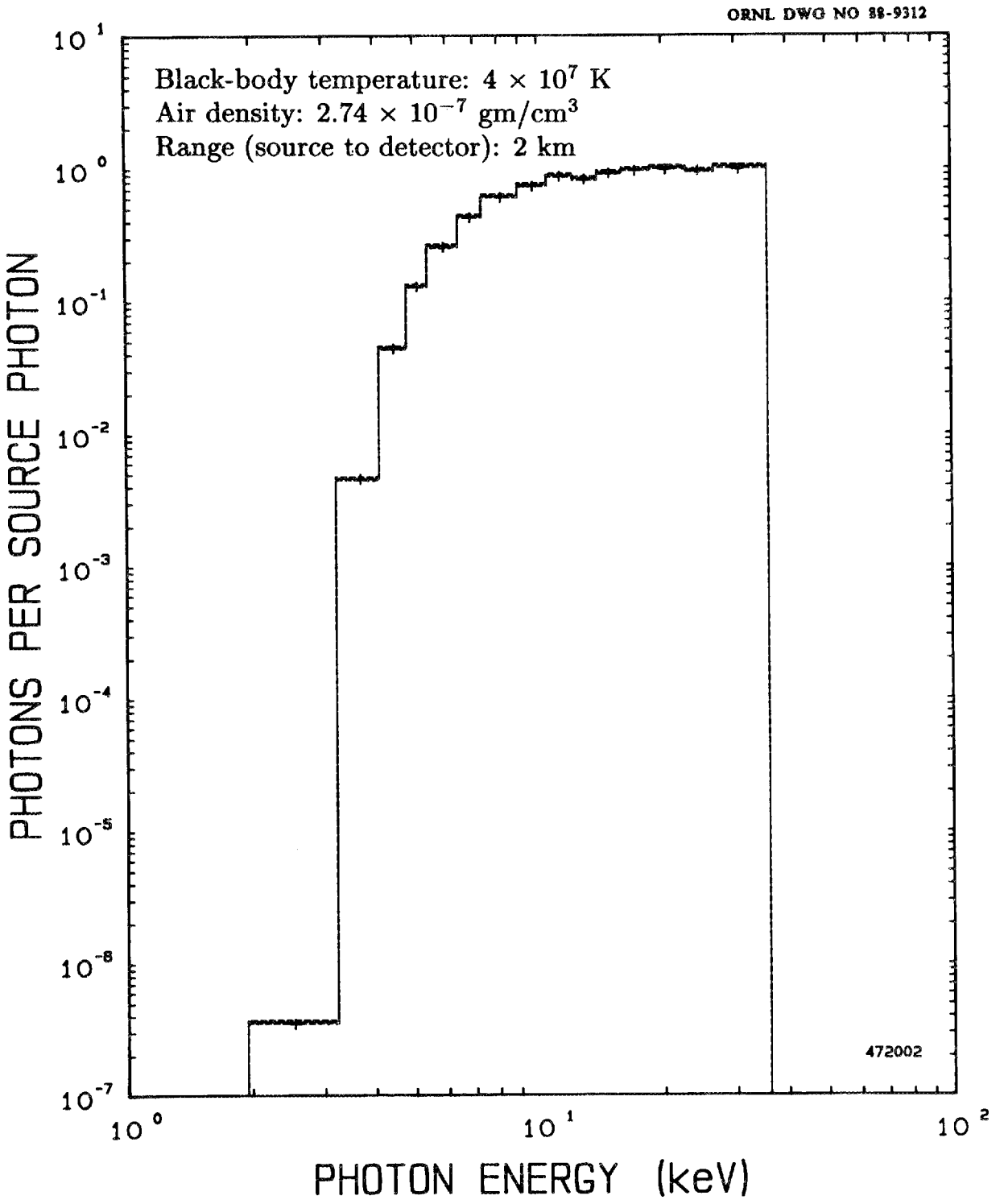

Figure 13. Detailed spectral comparisons of results from the approximation method (plus signs) with the Monte Carlo method (histogram with error limits indicated) for the case indicated on the figure.

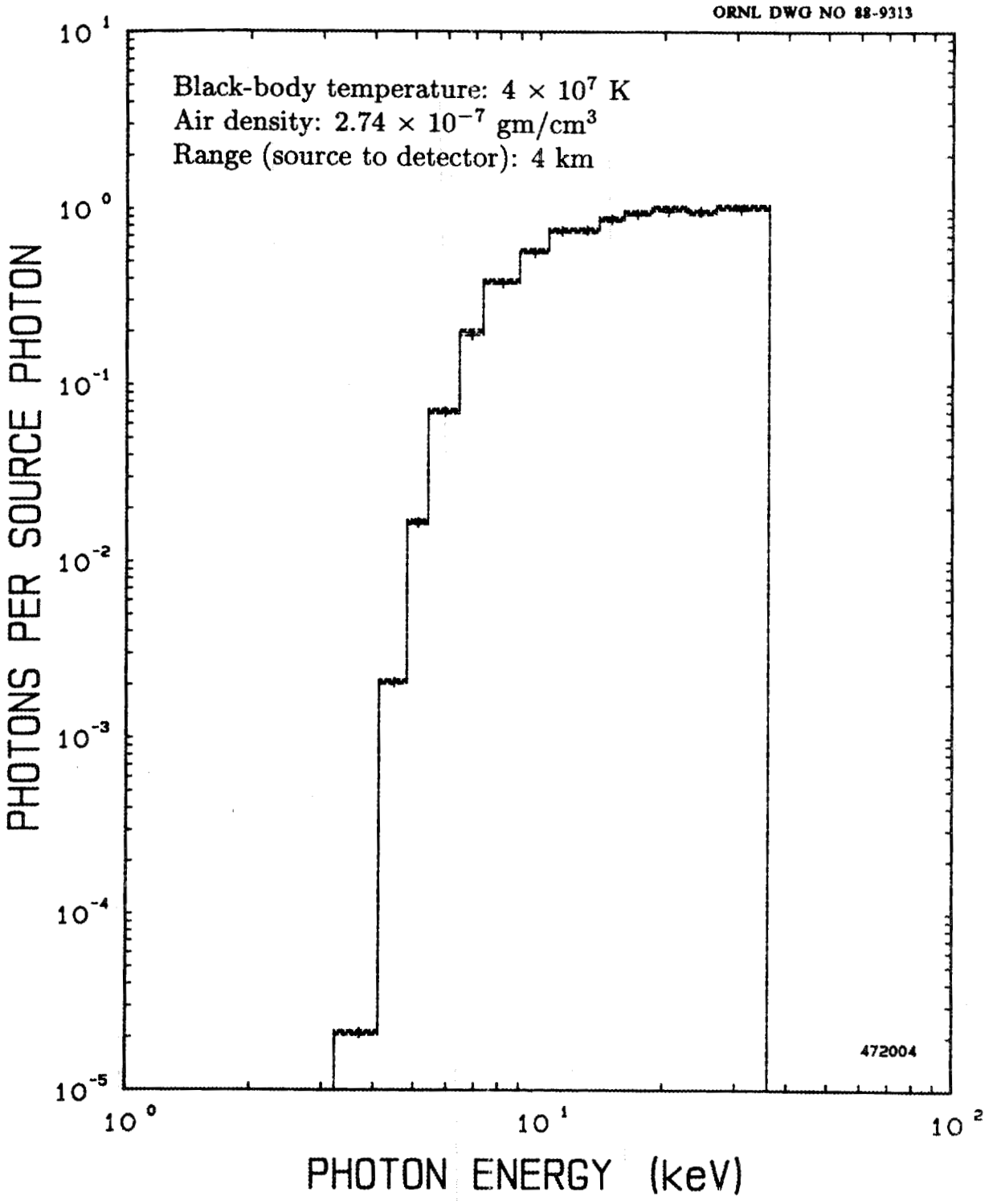

Figure 14. Detailed spectral comparisons of results from the approximation method (plus signs) with the Monte Carlo method (histogram with error limits indicated) for the case indicated on the figure.

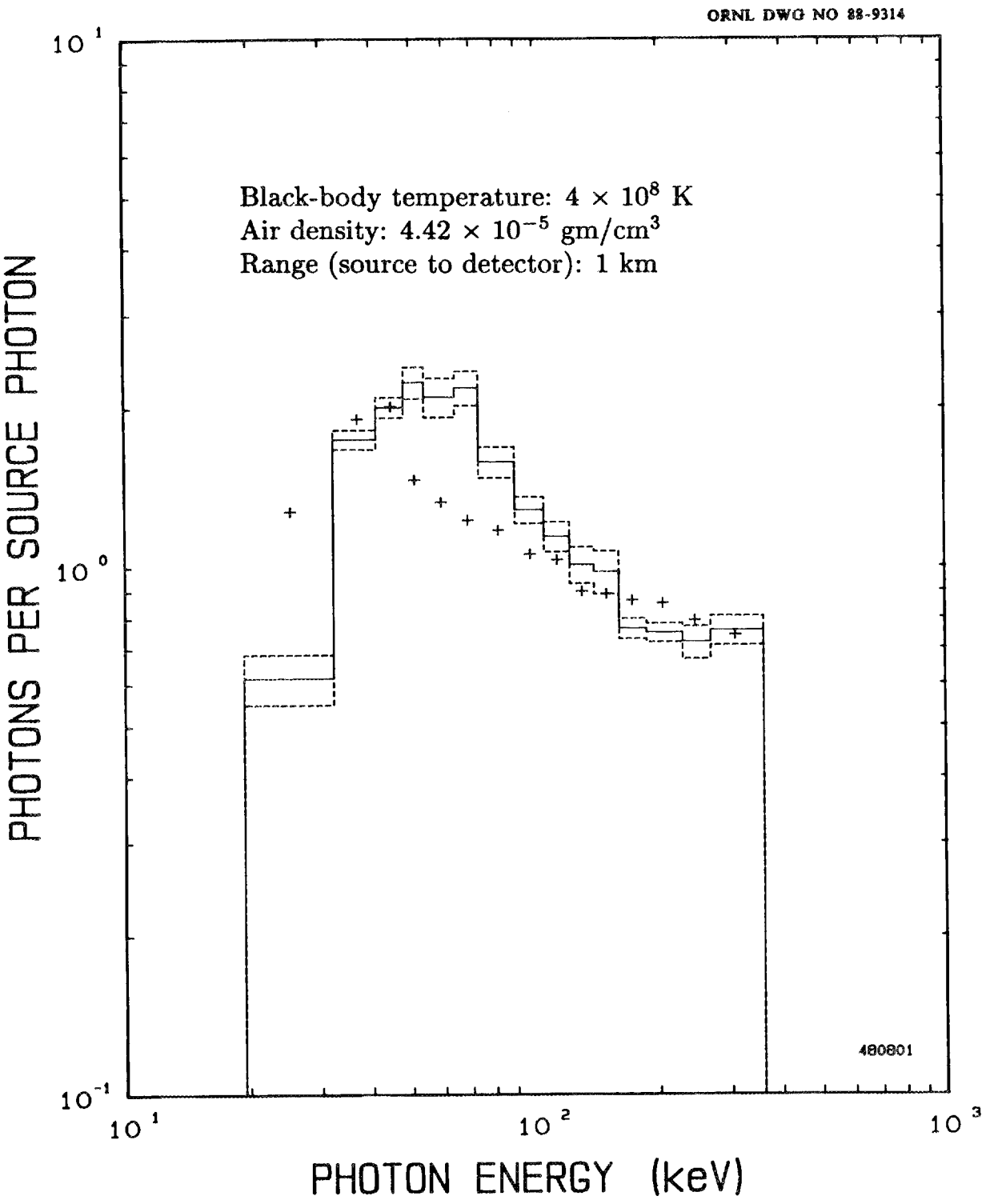

Figure 15. Detailed spectral comparisons of results from the approximation method (plus signs) with the Monte Carlo method (histogram with error limits indicated) for the case indicated on the figure.

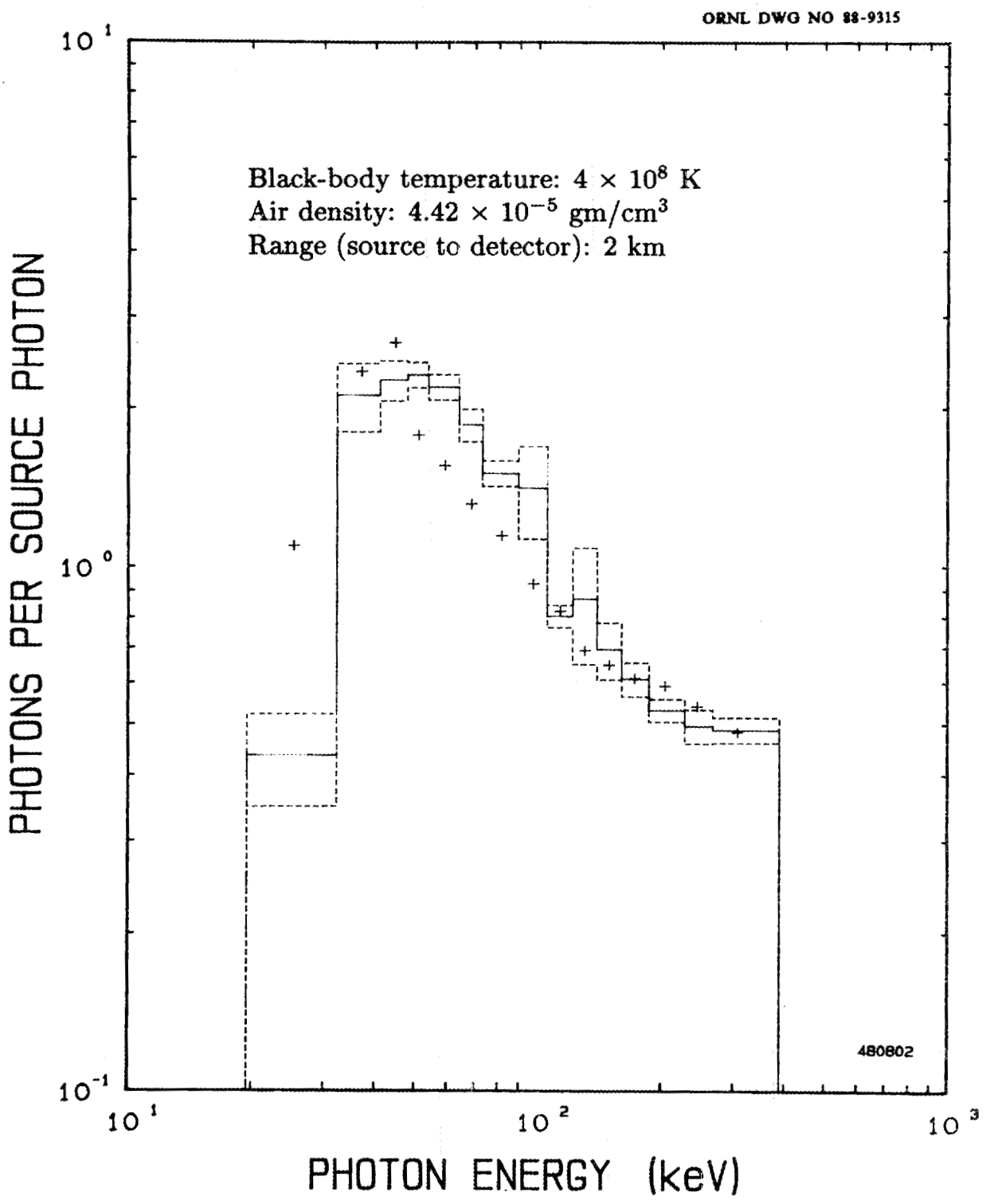

Figure 16. Detailed spectral comparisons of results from the approximation method (plus signs) with the Monte Carlo method (histogram with error limits indicated) for the case indicated on the figure.

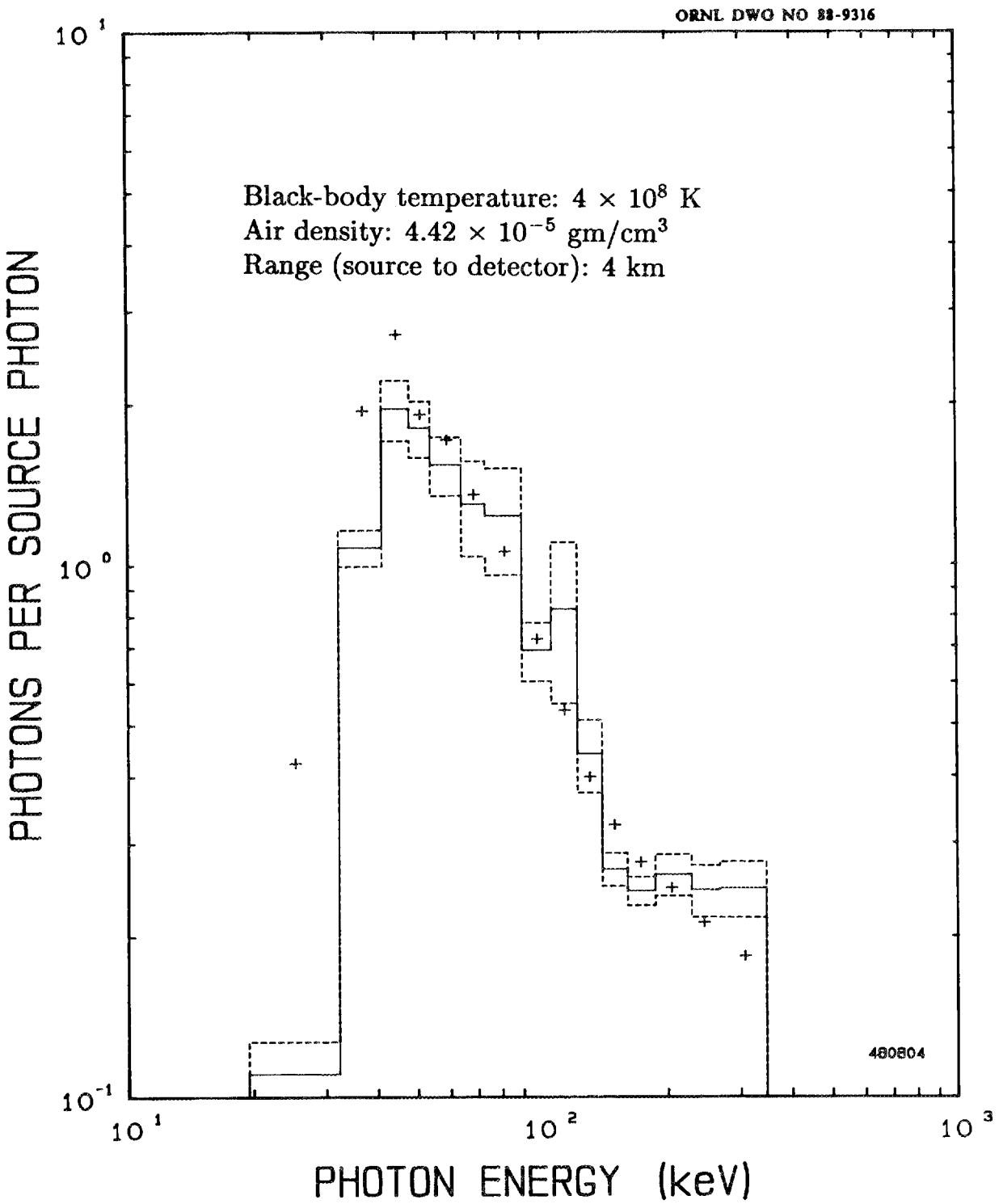

Figure 17. Detailed spectral comparisons of results from the approximation method (plus signs) with the Monte Carlo method (histogram with error limits indicated) for the case indicated on the figure.

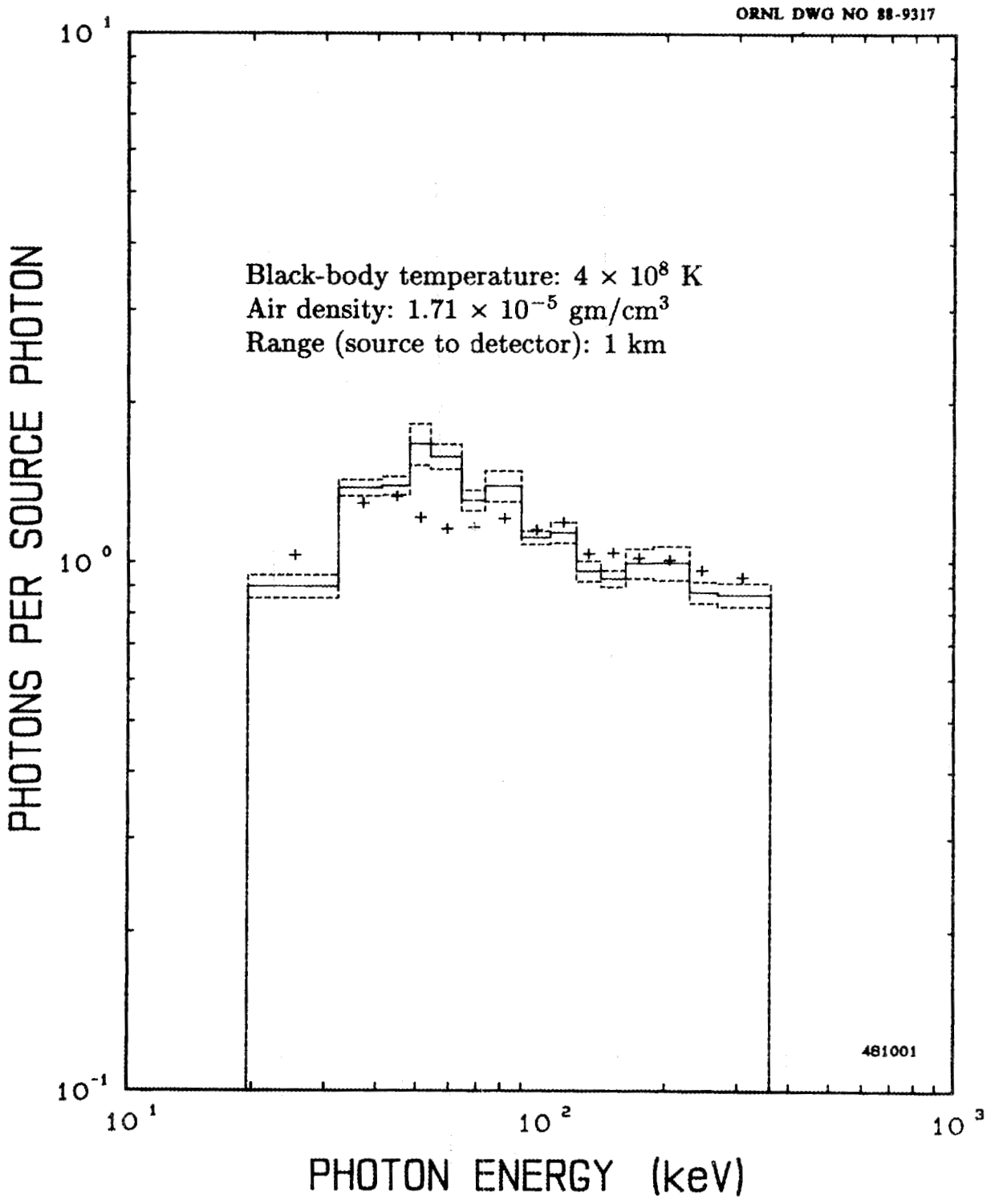

Figure 18. Detailed spectral comparisons of results from the approximation method (plus signs) with the Monte Carlo method (histogram with error limits indicated) for the case indicated on the figure.

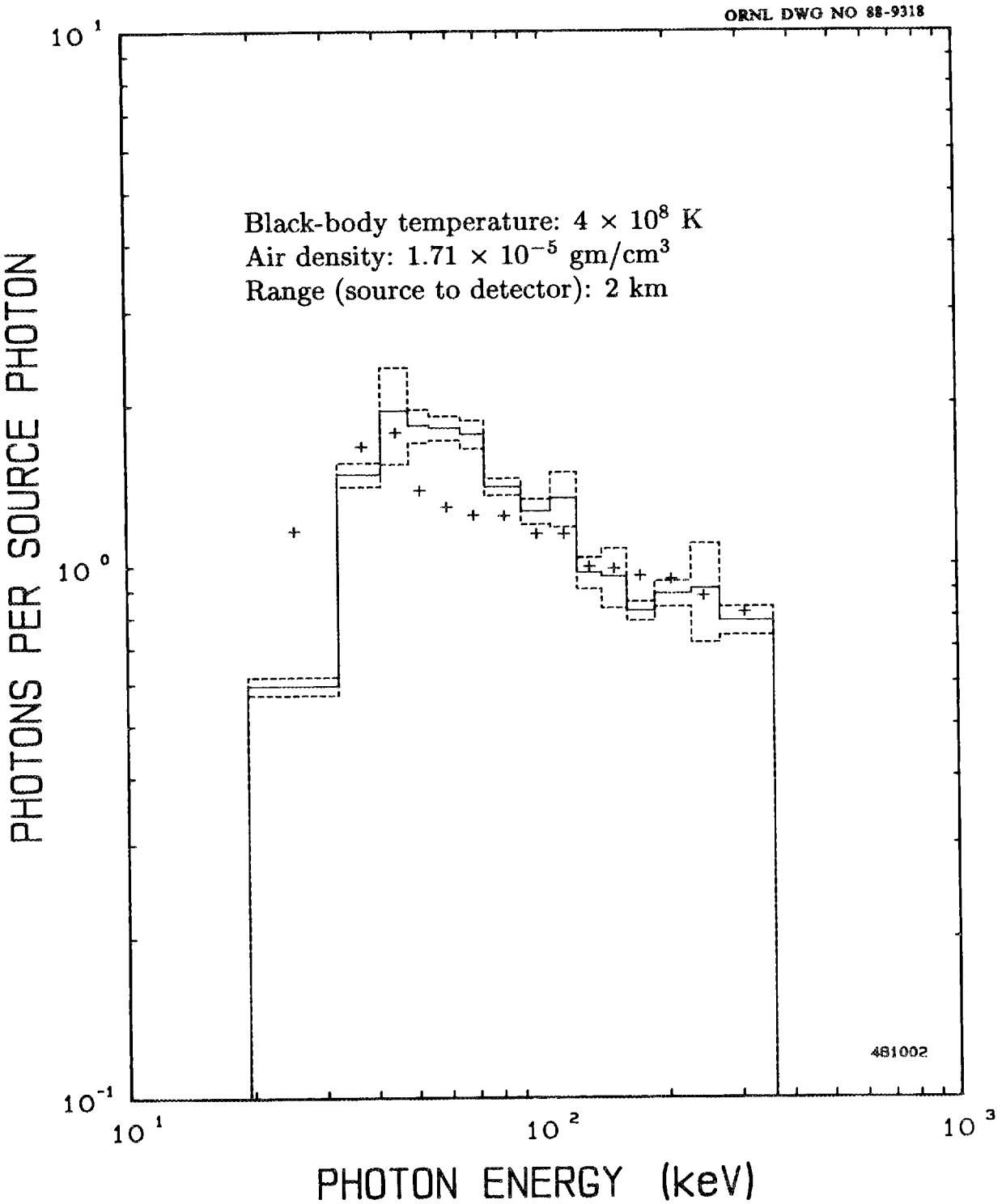

Figure 19. Detailed spectral comparisons of results from the approximation method (plus signs) with the Monte Carlo method (histogram with error limits indicated) for the case indicated on the figure.

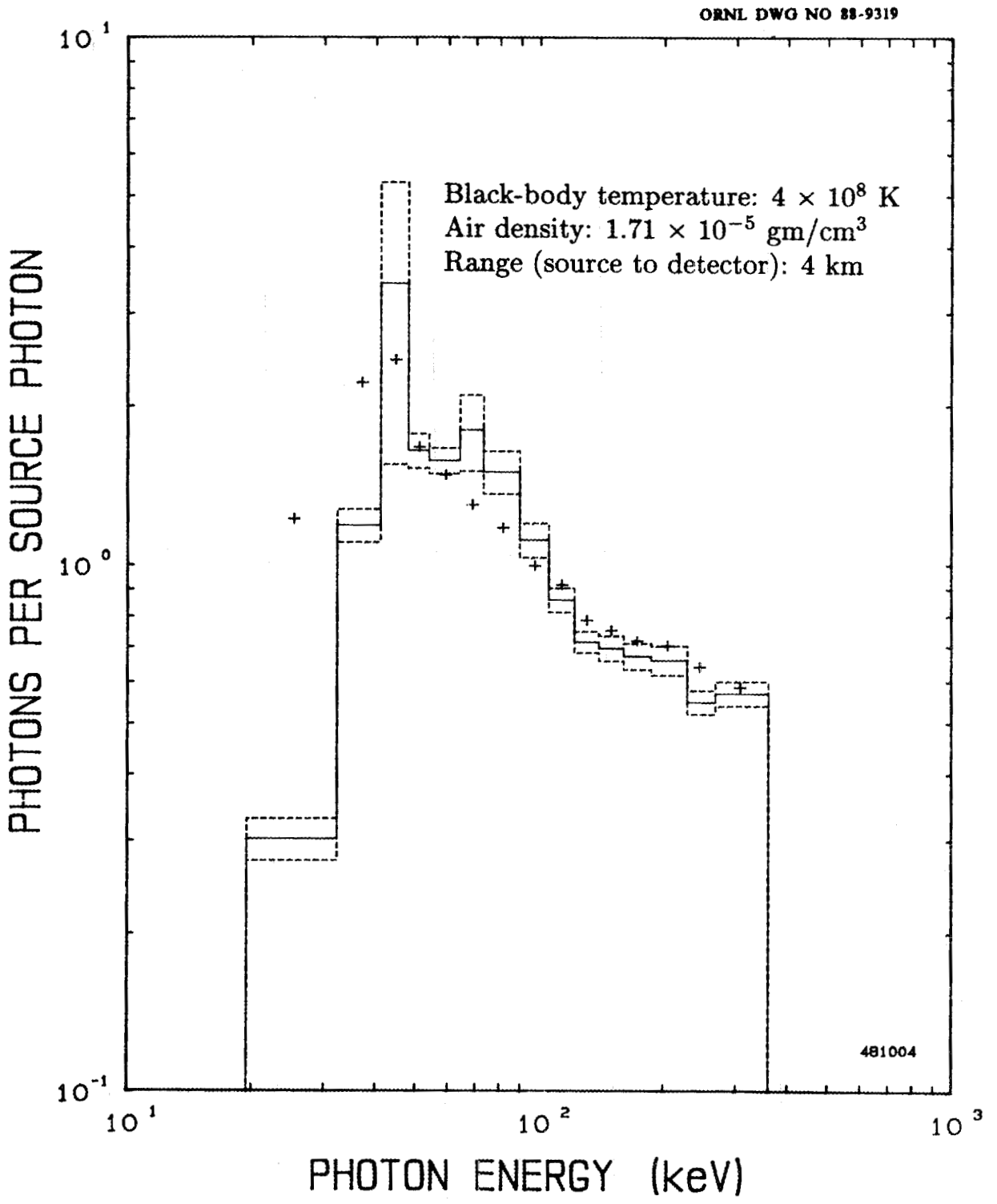

Figure 20. Detailed spectral comparisons of results from the approximation method (plus signs) with the Monte Carlo method (histogram with error limits indicated) for the case indicated on the figure.

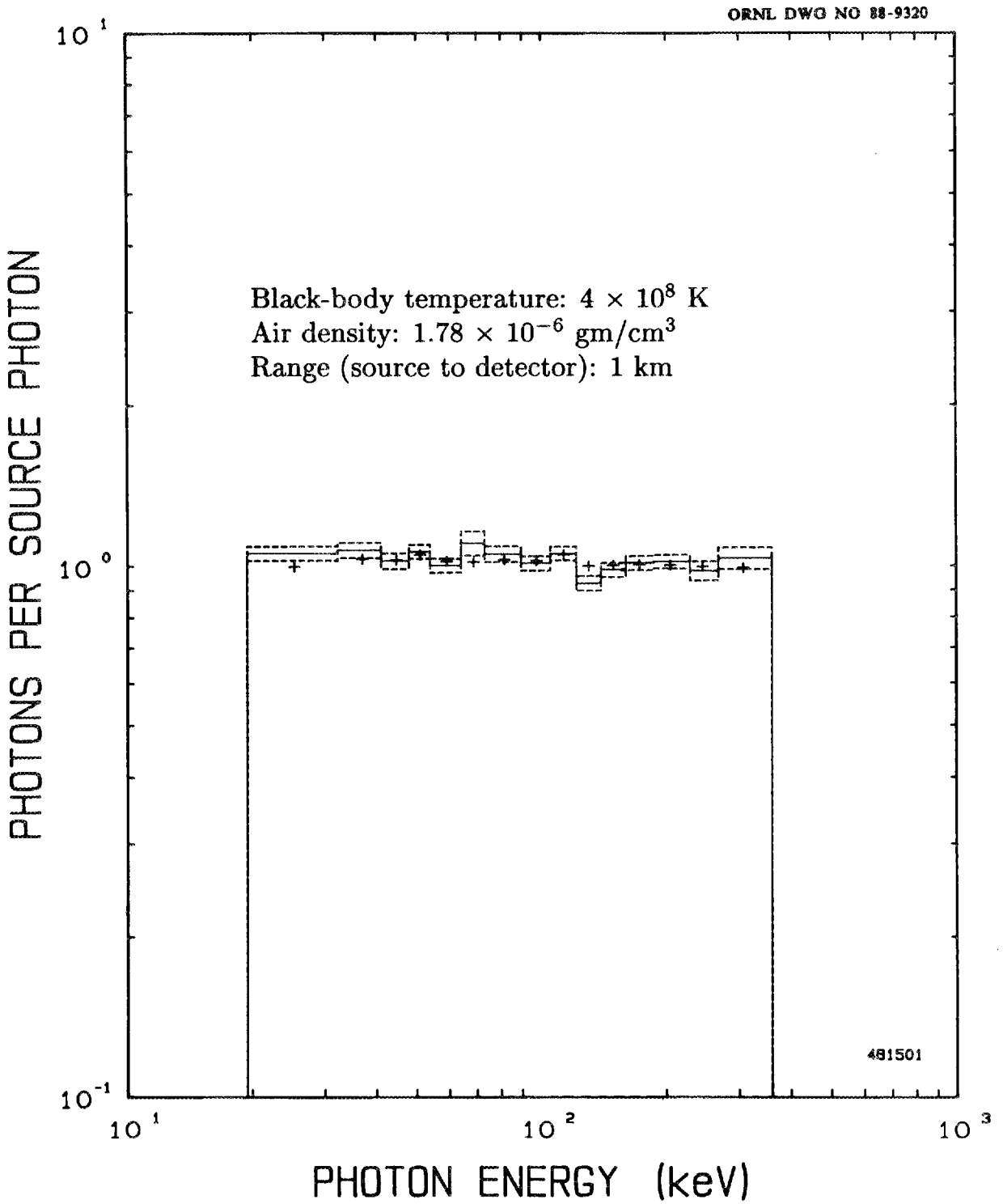

Figure 21. Detailed spectral comparisons of results from the approximation method (plus signs) with the Monte Carlo method (histogram with error limits indicated) for the case indicated on the figure.

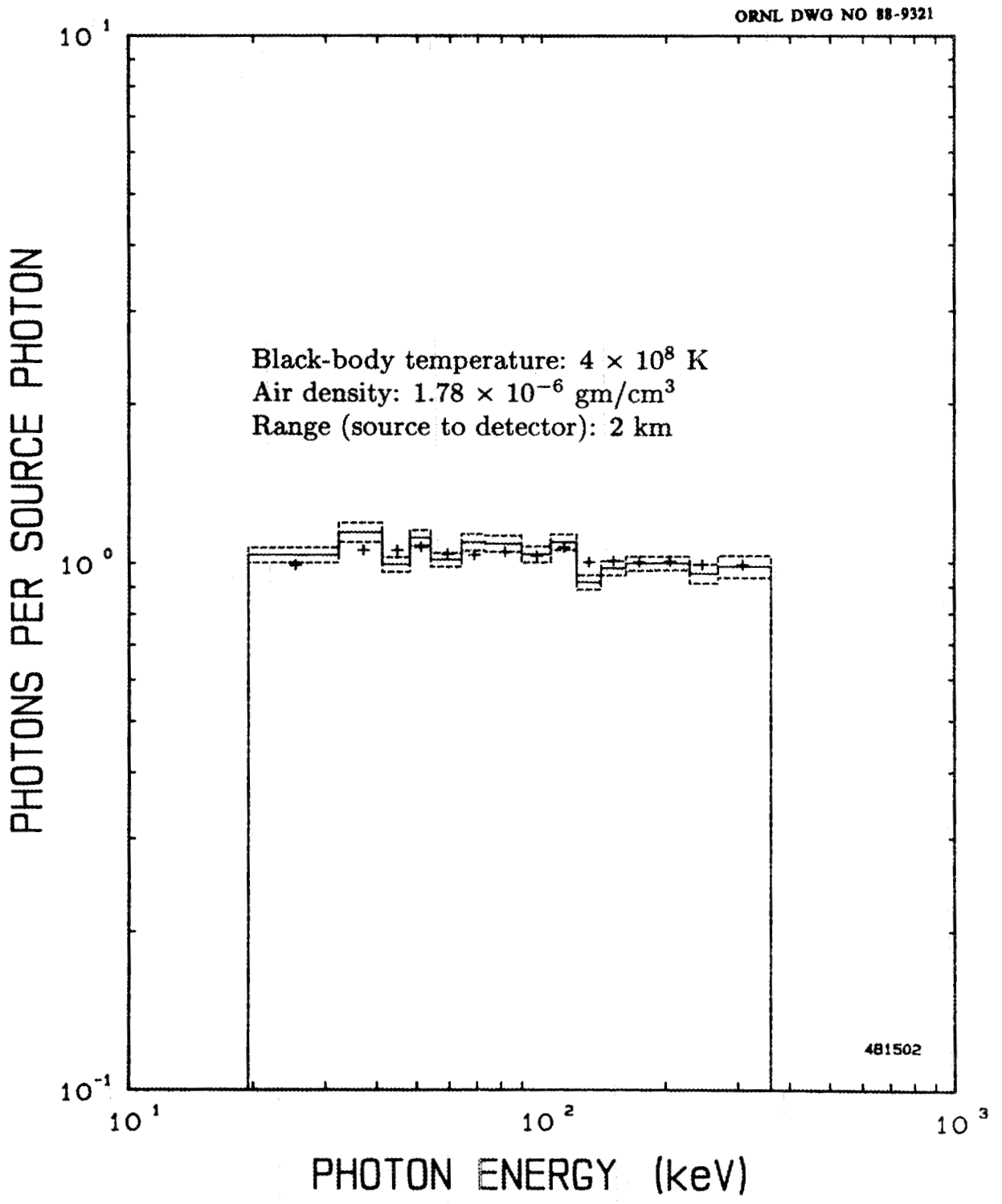

Figure 22. Detailed spectral comparisons of results from the approximation method (plus signs) with the Monte Carlo method (histogram with error limits indicated) for the case indicated on the figure.

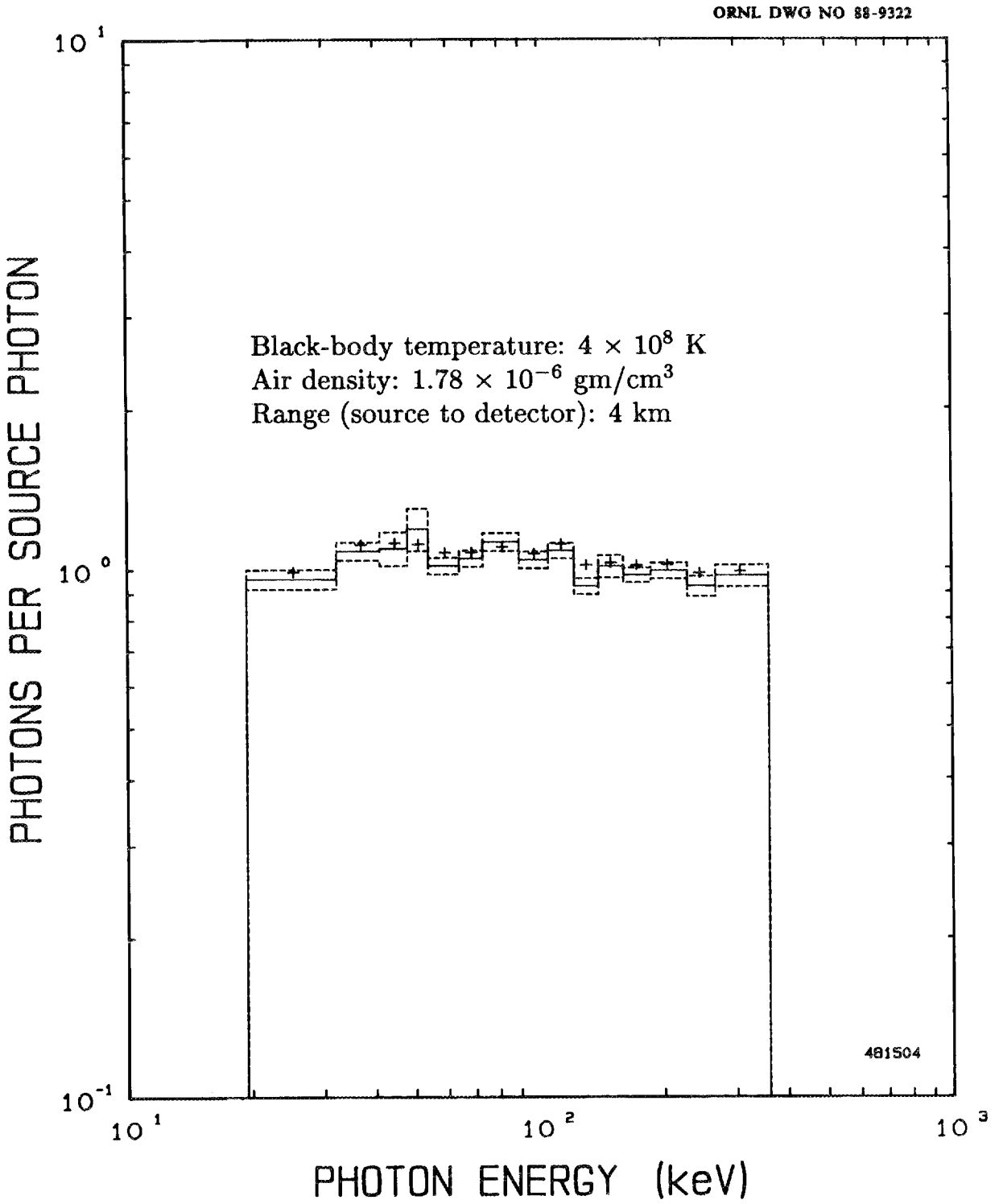

Figure 23. Detailed spectral comparisons of results from the approximation method (plus signs) with the Monte Carlo method (histogram with error limits indicated) for the case indicated on the figure.

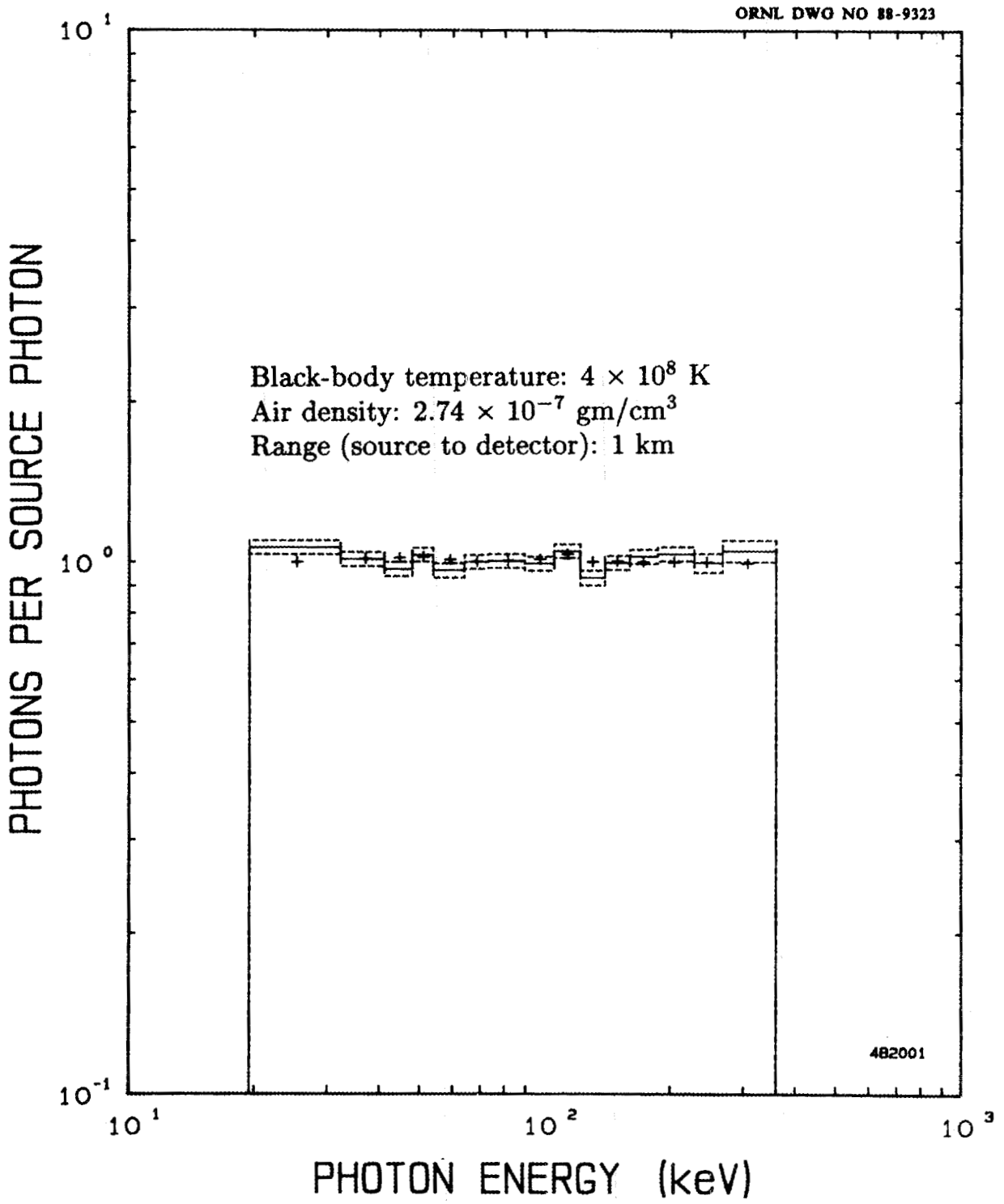

Figure 24. Detailed spectral comparisons of results from the approximation method (plus signs) with the Monte Carlo method (histogram with error limits indicated) for the case indicated on the figure.

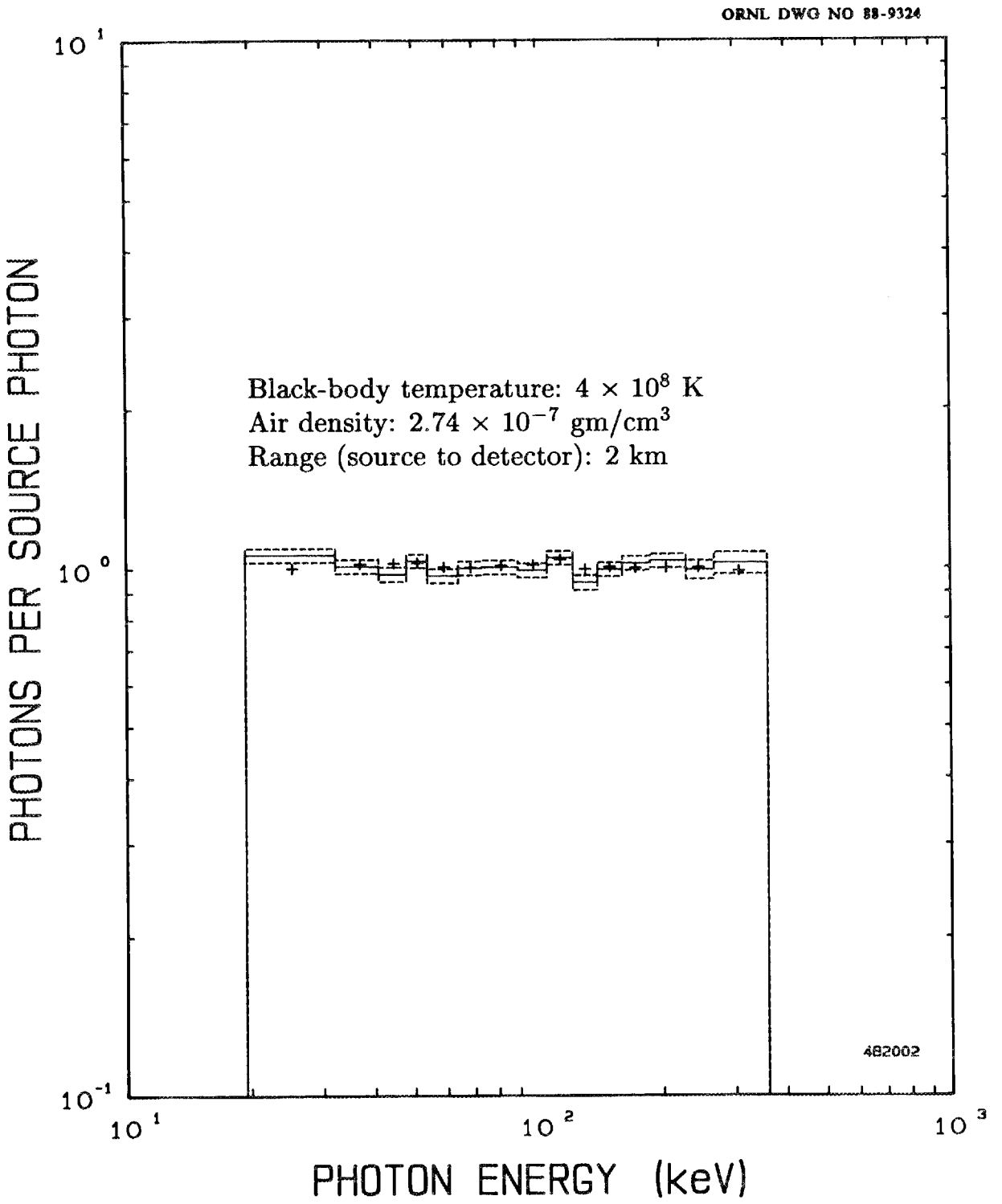

Figure 25. Detailed spectral comparisons of results from the approximation method (plus signs) with the Monte Carlo method (histogram with error limits indicated) for the case indicated on the figure.

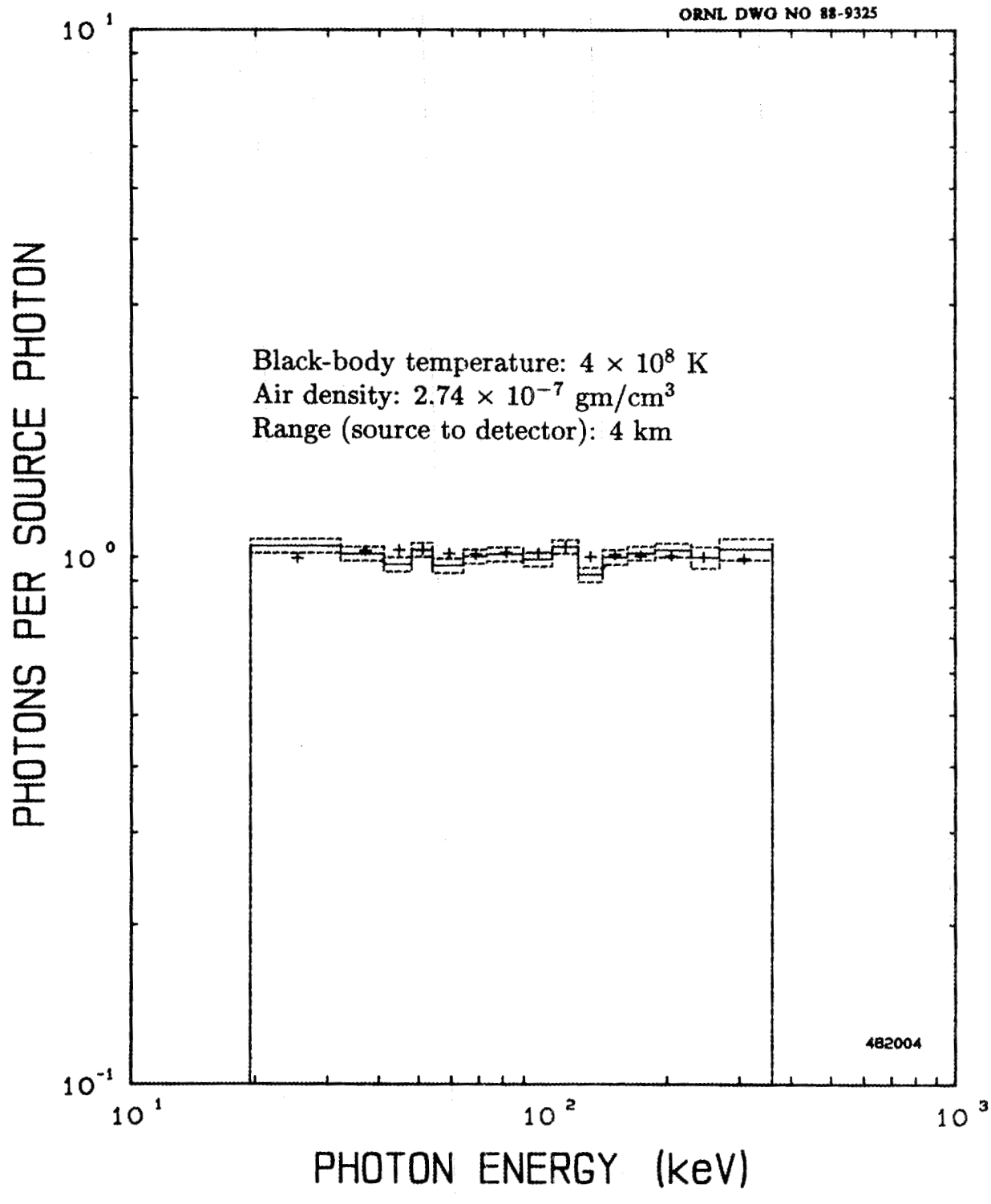

Figure 26. Detailed spectral comparisons of results from the approximation method (plus signs) with the Monte Carlo method (histogram with error limits indicated) for the case indicated on the figure.

At the lower atmospheric densities corresponding to 150 and 200 kft altitude, the number of mean free paths ranges from 0.004 to 0.2, consequently, absorption is negligible, as shown in Figures 15–26. For these cases, the statistical variations implicit in the Monte Carlo method show occasional small excursions from conservation of energy, the energy balance not being a factor in the MCNP program.

4. CONCLUSIONS

A simplified method and PC-based computer code were successfully developed which allows one to approximate to within about ± 10% the air transported x-ray spectrum from nuclear detonations in the atmosphere. The new code reduces the computational effort two to three orders of magnitude relative to the usual Monte Carlo-based computational approach. The new code will be especially valuable in conducting parametric studies of atmospheric attenuation wherein significant numbers of calculations may be required.

REFERENCES

1. S. Glasstone and P. J. Dolan (eds.), *The Effects of Nuclear Weapons*, 3rd Edition, (Washington, D.C.: Department of Defense and Department of Energy, 1977).

2. L. V. Spencer and U. Fano, *Physical Review* **81**, 464L (1951); also *J. Research National Bureau of Standards*, **46**, 446 (1951); and U. Fano, L. V. Spencer, and M. J. Berger, "Penetration and Diffusion of X-Rays," in *Handbuch der Physik*, **38/2**, S. Flugge (ed.) (Springer-Verlag, Berlin, 1959).

3. H. Goldstein and J. E. Wilkins, Jr., *Calculations of the Penetration of Gamma Rays*, NYO-3075, U.S. Atomic Energy Commission; and H. Goldstein, *Fundamental Aspects of Reactor Shielding* (Addison-Wesley, Reading, Massachusetts, 1959).

4. S. A. Dupree and H. A. Sandmeier, *Photon Transport Calculations Using the Method of Discrete Ordinates, Vol. I. Theoretical Considerations*, NWEF Report 1035—Vol. 1; AD-854805 (NTIS, 1969).

5. Judith F. Briesmeister, ed., *MCNP—A General Monte Carlo Code for Neutron and Photon Transport*, Version 3A, LA-7396-M, Rev. 2, Manual, also UC-32 (Low Alamos National Laboratory, 1986).

6. R. E. Lynch, J. W. Benoit, W. P. Johnson, and C. D. Zerby, *A Monte Carlo Calculation of Air Scattered Gamma Rays*, ORNL-2292, (Oak Ridge National Laboratory, 1958).

7. L. L. Carter, E. D. Cashwell, and R. G. Schrandt, *The Simulation of Low Energy Photon Transport and the Simulation of the Adjoint Neutron Transport Equation with Monte Carlo*, ORNL-RSIC-33 (Oak Ridge National Laboratory, 1971), pp. 197–207.

8. A. A. O'Dell, *Moments Method Calculation of the Scattered Angular Energy Flux for Point Isotropic Gamma Sources in an Infinite Homogeneous Air Medium*, EGG-1183-2275 (EGG, 1971).

9. C. J. Everett, E. D. Cashwell, and R. G. Schradt, *A Monte Carlo Transport Routine for the U.S. Standard Atmosphere (1962) to an Altitude of 90 Kilometers*, LA-5089; (Los Alamos National Laboratory, 1972).

10. A. B. Chilton, C. M. Eisenhauer, and G. L. Simmons, *Nuclear Science and Engineering* **73**, 97 (1980).

11. A. B. Chilton, J. K. Shultis, and R. E. Faw, *Principles of Radiation Shielding*, (Prentice-Hall, Inc., Englewood Cliffs, New Jersey, 1984).

12. J. H. Hubbell, *Int. J. Appl. Radiat. Isot.*, **33**, 1269 (1982).

INTERNAL DISTRIBUTION

1. R. G. Alsmiller, Jr.
2. B. R. Appleton
3. Y. Y. Azmy
4. D. E. Bartine
5–9. J. M. Barnes
10. R. B. Burditt
11. T. J. Burns
12. C. V. Chester
13. T. A. Gabriel
14. J. M. Googin
15–19. C. M. Haaland
20. R. L. Huddleston
21. D. T. Ingersoll
22. J. O. Johnson
23. H. E. Knee
24. F. C. Maienschein
25. J. V. Pace III
26. R. W. Peelle
27. R. W. Roussin
28–32. R. T. Santoro
33. M. S. Smith
34. D. G. Thomas
35. D. K. Trubey
36. C. R. Weisbin
37–38. EPMD Reports Office
39–40. Laboratory Records Department
41. Laboratory Records, ORNL–RC
42. Document Reference Section
43. Central Research Library
44. ORNL Patent Office

EXTERNAL DISTRIBUTION

45. Dr. John J. Dorning, Department of Nuclear Engineering and Engineering Physics, Thornton Hall, University of Virginia, Charlottesville, VA 22901
46. C. Fawcett, AFWAL/FIBA, Air Force Wright Aeronautical Laboratory, Wright-Patterson Air Force Base, Ohio 45433-6553
47. J. N. Garrison, AFWAL/FIBA, Air Force Wright Aeronautical Laboratory, Wright-Patterson Air Force Base, Ohio 45433-6553
48. Dr. Robert M. Haralick, Department of Electrical Engineering, University of Washington, Seattle, Washington 98195
49. J. H. Hubbell, National Bureau of Standards, Gaithersburg, MD 20899
50. P. Lane, AFWAL/FIBA, Air Force Wright Aeronautical Laboratory, Wright-Patterson Air Force Base, Ohio 45433-6553
51. L. V. Spencer, Post Office Box 87, Hopkinsville, Kentucky 42240

52–54. S. D. Thompson, AFWAL/FIBA, Air Force Wright Aeronautical Laboratory, Wright-Patterson Air Force Base, Ohio 45433-6553

55. CPT D. M. Topa, AFWL/NTW, Air Force Weapons Laboratory, Kirtland Air Force Base, New Mexico 87117-6008
56. Office of Assistant Manager for Energy Research and Development, Department of Energy, Oak Ridge Operations Office, P.O. Box E, Oak Ridge, Tennessee 37831

57–66. Office of Scientific and Technical Information, P.O. Box 62, Oak Ridge, Tennessee 37830